Miniaturized conductivity measurement system

I. Anastasopoulos

for in-situ water quality management

TU Delft

Miniaturized
conductivity measurement system

by

I. Anastasopoulos

to obtain the degree of Master of Science
at the Delft University of Technology,
to be defended publicly on Tuesday January 1, 2013 at 10:00 AM.

Student number:	4502388	
Project duration:	February 14, 2017 – October 31, 2017	
Thesis committee:	Prof. dr. PJ. French,	TU Delft, supervisor
	Dr. G. de Graaf,	TU Delft
	Dr. AJ. van Genderen,	TU Delft

This thesis is confidential and cannot be made public until February 15, 2021.

TU Delft

Preface

Fresh water is becoming rarer by time. Many countries in order to deal with this problem are mixing fresh with saline water for irrigation purposes. Some are using treated waste water coming from domestic, industrial and animal production that is also high in salt concentration. The massive draining of underground water in collaboration with the rise of sea level has led to the contamination of those deposits with saline water. It is found that the use of water with conductivity in irrigation is suboptimal in terms of the yield and quality crops.

This problem has led to an increased interest from the growers' side on a fast, low cost, on site and reliable method of determining the conductivity of water that they intent to use for watering their crops. The results of the application can help developing countries to maximize their production given the resources available to them.

This document describes the work which was carried out for the MSc Thesis Project, as part of the MSc Embedded Systems. This project is done in collaboration with SODAQ.

The objective of this project is the development of a conductivity sensor that fulfils the following criteria:

- Accuracy
- Wide value spectrum
- High resolution
- Portability
- Durability through time
- Ease of use

During the course of this work, many techniques are studied and evaluated. The electrical conductivity measurement technique is the one found to meet the above criteria in the best way. After that, an initial proof of concept takes place with the equipment available at that time. Then various different probe designs are simulated and studied in order to select the one that will be implemented. The behaviour of the probe relevant to the work is then studied. The results of those simulations are then used in order to find the calibration curve that will allow the conversion from the measured conductance to the conductivity of the medium.

At this point I would like to express my gratitude Ger de Graaf for his daily supervision as well as his valuable guidance throughout the course of the whole project and his comments and suggestions. I would also like to thank Itay Dagan from SODAQ for his assistance and facilitation through the project. Another very important contributor to the project that I owe to thatnk is Nick Leijenhorst, whose assistance and input was critical to the completion of the project. I would also like to thank Guido Sturm for his assistance during a measurement session and a valuable conversation.

Lastly, I would like to thank my colleague and dear friend Efthymios Giannopoulos, for his help throughout the whole journey of our master program.

I. Anastasopoulos
Delft, January 2018

Contents

1

Problem Statement

Estimations show that by 2025 the scarcity of fresh water will affect 60% of the total population. Large parts of the world are already facing the problem. Most of the countries, in order to deal with this problem are either mixing fresh water with sea or saline water and some recycle already used water [22].

The introduction of NaCl in irrigation water has a negative impact on the various crops according to Table 1.1 [5] .

Crop	Threshold salinity level without growth and/or yield reduction	Yield decrease (%) per unit EC increase	EC (mS/cm) at which 10% yield is lost	EC (mS/cm) at which 25% yield is lost
Horticulture				
Cucumber	1,7	20,8	2,2	2,9
Lettuce	0,9	20,8	1,4	2,1
Melon	1,5	10,9	2,4	3,8
Potato	1,1	17,9	1,7	2,5
Sweet pepper	1	20,8	1,5	2,2
Tomato	1,7	14,7	2,3	3,4
Fruits				
Apple	1	20,8	1,6	2,2
Avocado	0,9	33,3	1,2	1,7
Banana	0,5	41,7	0,7	1,1
Orange	1,1	21,7	1,6	2,2
Strawberry	0,7	50	0,9	1,2

Table 1.1: Examples of EC tolerances of various crops

The knowledge of the conductivity of water is significant in large parts of the planet, where the access to fresh irrigation water or irrigation water, with high standards is limited. For example in parts of Africa or Asia, the conductivity of the used irrigation water can make a great difference in the yield of an individual farmer, his/her family income and the rest of the community.

Any individual farmer needs to have an informed opinion on whether the water available has conductivity falling within the tolerance boundaries of each specific crop. In order to do that, the farmer needs an easy-to-use, measurement equipment that can be employed on-site and provide results of high confidence.

Today there seems to be trade-offs between mobility, confidence in measurement and price. Accurate measurements require expensive lab equipment in order to provide reliable results, but they suffer in terms of time and complexity and they are definitely unavailable for on-site use. On the other hand commercially available hand-held or, more generally, mobile devices can be expensive or suffer greatly from inaccuracies

and their performance changes over time due to (re-)calibration and maintenance needed for mobile devices that makes them unreliable in the scope of time.

The system described in this report, can provide the users with reliable measurements, through a simple user interface. The calibration necessary for this sensor is a very simple and straight-forward process, requiring minimum user effort.The standards of the system are the following:

The range of measurement of the system is between 0 and 20.000 μS (20 mS).

The desired accuracy is under 10%, through that spectrum of conductivity values.

2

State of art techniques

This chapter describes different methods used in order to define the conductivity of water. The physical principals behind each method are discussed, as well as the different measurement principals.

2.1. Optical Method

2.1.1. Physical Principal

When a ray of light changes the medium through which it propagates under an angle θ_1, if the cross-section surface is flat and smooth, two phenomena take place: reflection and refraction. This means that a part of the energy of the light gets reflected back to the medium where it came from and another part gets through the cross-section surface. As it is shown in Figure 2.1 the angle of reflection is the same as the angle of incidence.

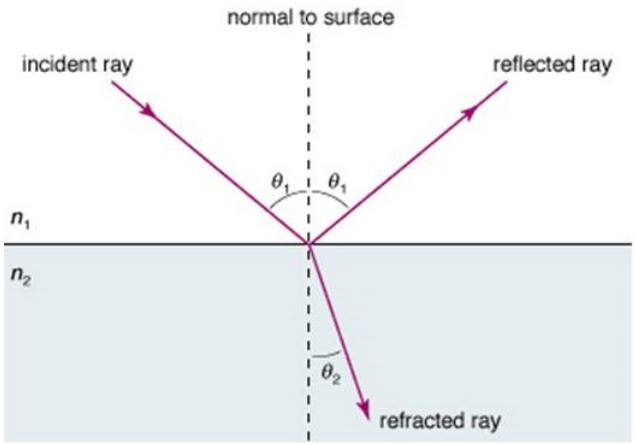

Figure 2.1: Reflection and refraction

The part of the energy that got through to the next medium is refracted in accordance to the Snell's law:

$$\frac{sin\theta_1}{sin\theta_2} = \frac{n_2}{n_1}$$

where:

θ_1 is the angle of the incident ray,

θ_2 is the angle of the refracted ray,

n_i is the unit-less refractive index of the each medium.

The refractive index of the medium depends both on the kind of light (wavelength) that is directed to a medium (colour dispersion), as well as the qualities of the medium.

More specifically the index of refraction of a medium is the ratio between the speed of light in vacuum and the speed of light in that medium:

$$n = \frac{c}{v_p}$$

where:

c is the speed of light in vacuum and

v_p is the speed of light on the specific medium.

It is known from electromagnetism that:

$$c = \sqrt{\frac{1}{\epsilon_0 \mu_0}}$$

$$v_p = \sqrt{\frac{1}{\epsilon \mu}}$$

where:

ϵ_0 is the electromagnetic permittivity of vacuum,

μ_0 is the electromagnetic permeability of vacuum,

ϵ is the is the permittivity of the medium,

μ is the permeability of the medium.

Using the above two equations it is found that:

$$n = \sqrt{\epsilon_r \mu_r}$$

where:

ϵ_r is the relative permittivity or dielectric constant and

μ_r is the relative permeability.

For non- magnetic mediums (such as salt-water) μ_r is almost 1, so the previous equation can become:

$$n \approx \sqrt{\epsilon_r}$$

By adding salt into water the dielectric constant increases, increasing the refraction index of water. According to [46] there is linear relation between the salinity of the water and the refraction index as it can be seen in Figure 2.2:

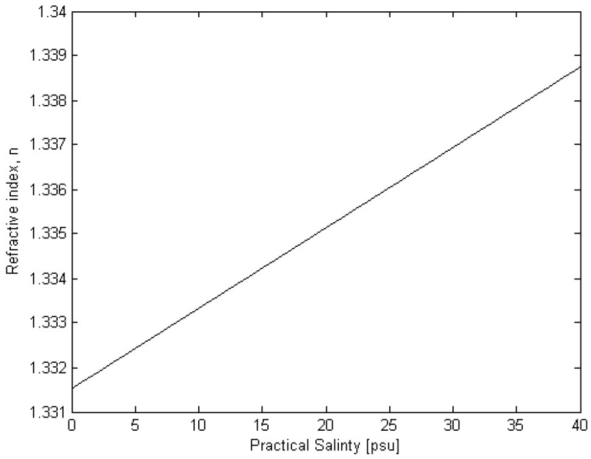

Figure 2.2: Refractive index as a function of salinity (1psu=1g/kg)

Both [46] and [45] suggest that temperature has a significant influence in the measurement. Although [45] does not go into details about this relation, they compensate their values due to temperature being different from $25^{o}C$. [46] provides a curve of the relationship between the temperature and the refractive index.

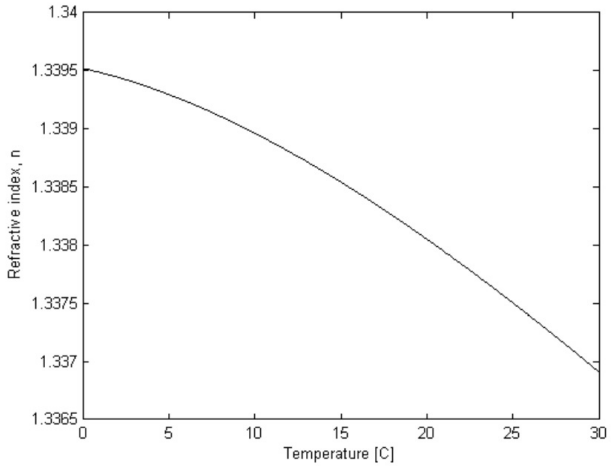

Figure 2.3: Refraction index as function of Temperature

[46] studied the implications of pressure on the measurement of the refractive index. The results of his study are shown in Figure2.4

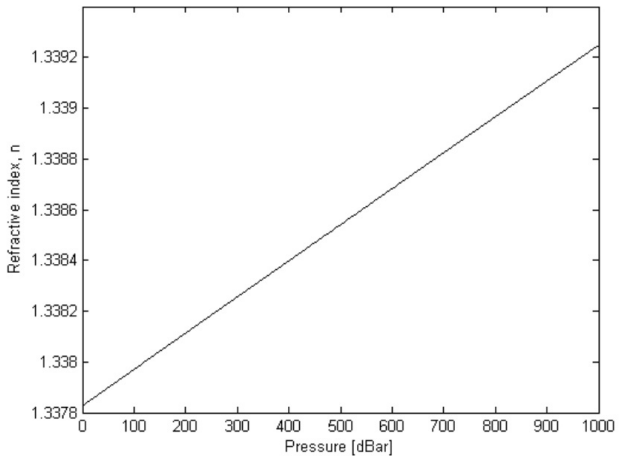

Figure 2.4: Refraction index as function of pressure

The linear coefficient in this graph is $14*10^{-7}$ $dBar^{-1}$ and so it can easily be neglected for most environmental measurements.

2.1.2. Refractometer

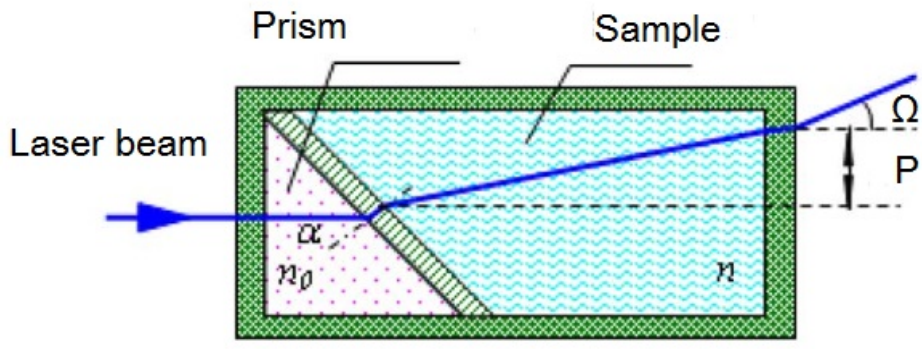

Figure 2.5: Refractometer cell

A simple refractometer is described in [45]. A refractometer on its most basic form exploits the light refraction phenomenon in order to define the refraction index of a sample and from that to define its salinity. As it is described in the [45] and shown in Figure 2.5 a laser beam is directed perpendicularly to a triangle prism of known refraction index. On the other side of the prism the sample under examination is placed. The relationship between the two refraction indexes can be described from the following relationship:

$$\Delta n = n - n_0 = \Omega cot\alpha + \frac{\Omega^2}{2n} \approx kP$$

where:

n is the refraction index examined,

n_0 is the refraction index of the prism,

α is the incidence angle of the laser beam and the surface of the prism,

Ω is the exit angle and

k is a constant dependent on the geometrical characteristics of the device.

The basic concept of a more advanced digital refractometer is shown on Figure 2.6

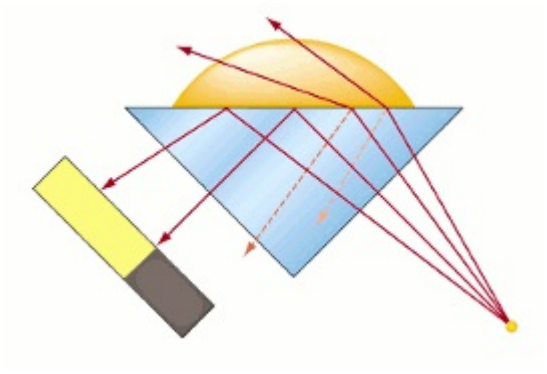

Figure 2.6: Digital Refractometer cell

Uncollimated light source is used instead of laser. This is due to the fact that laser is heavily directional and focused, meaning that the beam will either be totally internally reflected or it will pass to the medium. This light source is directed to the triangular prism that has a high refractive index. On the one side of the prism, the sample under examination is placed. If the angle of incidence of a beam of the light source exceeds

a certain value the light is internally reflected back to the prism. This light is detected by the CCD sensor. According again to Snell's law the lower the refractive index of the sample, the smaller the critical angle becomes and the bigger the illuminated area of the sensor becomes. So the refractive index can be found from the ratio of the illuminated and the dark area of the CCD sensor.

Refractometry is widely used among brewers and aquarium hobbyists. Both those categories are interested in measuring the refraction index of samples: the first ones are interested in measuring the sugars and alcohol in their beer or wine collection, while the later are more interested in measuring the salt concentration inside their aquariums in order to make sure that their fishes are living under the proper conditions.

Most of the refractometers use Brix as a measurement unit, which corresponds to 1 gram of sucrose in 100 grams of solution. Table B.1 showing the correlation between Brix Refraction index and salt found in [41] can help in conversions.

A simple refractometer that does not take into account temperature's influence on the measurement costs around 20 to 40 €. The sensitivity at this price range is usually ±0.5% Brix which translates to ±4g/kg according to Table B.1. According to [11] sea water that has a concentration of 35g/kg has a conductivity of 3.27 S/m. Supposing that the relation between salinity and electrical conductivity is linear the above mentioned error translates 0.6 S/m. Such error makes those refractometers unfit candidates for accurately measuring the salinity.

There are more sophisticated refractometers that have smaller error measurement and take into account the temperature in their measurement, but usually cost over 200 €.

2.2. Specific Gravity

2.2.1. Physical principal

Specific gravity is the ratio between the density of the studied sample and a reference sample. Due to the fact that it is a ratio of densities it is unitless. For solids and liquids the reference substance is usually pure water while for gazes is usually air ([26], [25]). Those reference densities are given for a specific value: for water that value is usually 4^oC, as at that temperature water has its maximum density ($1kg/m^3$), and for air it is usually 21^oC.

Specific gravity is used to characterize substances, with the use of tables that contain values for the specific gravity of common substances. Specific gravity is thus heavily dependent on the composition of the samples examined as well as in the temperature. In Figure 2.7, taken from [37], they examine the samples taken from oilfield waters around the world. The results of their measurement reveal a linear relationship between the specific gravity of water and the salinity.

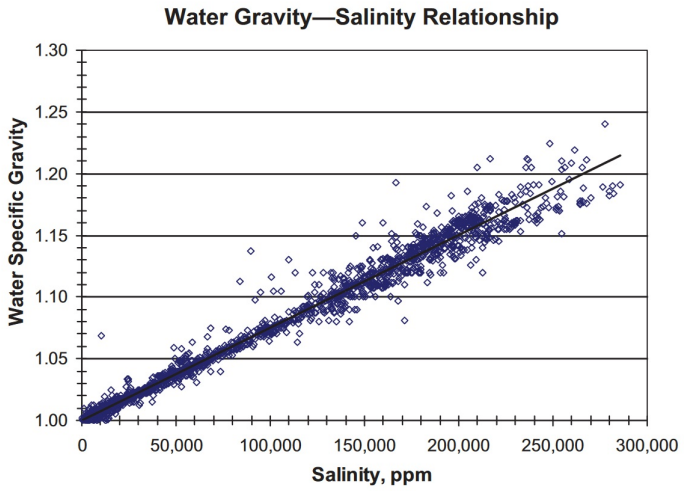

Figure 2.7: Water Specific Gravity-Salinity relationship

In [25] can be found a definition of chlorinity at page 10. There it is stated that chlorinity is the "number of grams of atomic weight silver necessary to precipitate the halogens in 0.3285234 kg of sea water".

At the same book at pages 25-26 there is a more thorough description of the relationship between specific

gravity, chlorinity and salinity, as well as a description of the relationship between specific gravity, temperature and density of the sample.

Those relationships are derived from curves made to fit the data collected and they do not have a lot of physical information about the exact relations of the different quantities.

$$\sigma_0 = \sigma_0(S), S = S(Cl)$$

$$S = 0.030 + 1.8050Cl$$

The first two equations suggest that specific gravity at 0^oC is a function of salinity and that salinity itself is a function of chlorinity. Next there is the relationship between salinity and chlorinity:

$$\sigma_0 = -0.069 + 1.4708Cl - 0.001570Cl^2 + 0.00000398Cl^3$$

(As it can be seen the prevailing term is the linear one, since the factors of higher order are significantly smaller. This equation can also explain the results shown in Figure 2.7, where for low salinity the data points appear to follow the line, while for increasing salinity there is a notable divergence from the line.)

$$\sigma_T = \sigma_T(\sigma_0, T)$$

The above equation denotes that the specific gravity, at a temperature T, σ_T is a function of the specific gravity at 0^oC and the temperature. The empirical mathematical formula describing exactly this relation is:

$$\sigma_T = \Sigma_T + (\sigma_0 + 0.1324)\left[1 - A_T + B_T(\sigma_0 - 0.1324)\right]$$

where:

σ_0 is the specific gravity of water at 0^oC,

S is the salinity,

Cl is the chlorinity,

σ_T is the specific gravity at temperature T,

$$\Sigma_T = -\frac{(T-3.98)^2}{503.570}\frac{T+283}{T+67.26}$$

$$A_T = T(4.7867 - 0.098185T + 0.0010843T^2)10^{-3}$$

$$B_T = T(18.030 - 0.8164T + 0.01667T^2)10^{-6}$$

There are many different instruments and methods in order to measure the density and finally the specific gravity of a substance.

2.2.2. Hydrometer

One of the most common is the pychnometer or hydrometer. The key principal behind the measurement is Archimedes' principal. According to that a body suspended in a fluid experiences a force named buoyancy. The amount of the force is equal to the weight of the fluid displaced by the part of the body under the surface of the fluid.

Figure 2.8 shows how a typical hydrometer is used: The fluid that is under examination is placed in a cylindrical vessel (a graduated cylinder for example). Depending on the ratio between the densities of the fluid examined and the fluid enclosed in the hydrometer the latter will be submerged as deep as Archimedes' principle dictates. The scale in the stem of the hydrometer provides the user with the measurement of the specific gravity.

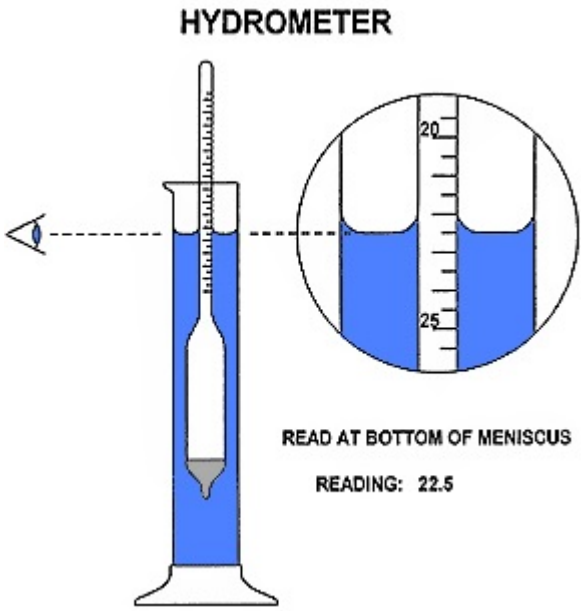

Figure 2.8: Typical hydrometer in measurement set-up

A hydrometer can cost as low as 4 €, but the measurement is of very low accuracy.

2.2.3. Hydrostatic Pressure

Another way to measure the special gravity of a solution is by measuring the hydrostatic pressure difference between two points of different height of the fluid. Pascal's principle dictates that:

$$\Delta p = \rho \alpha \Delta h$$

where:

Δp is the hydrostatic pressure difference between two points at different height,

ρ is the density of the substance,

α is the acceleration experienced from the fluid, on earth it would be the acceleration of gravity α=g=9.80665 m/s^2 and

Δh is the height difference between those two points.

By measuring the pressure in two different heights, the density of the fluid can be calculated and from there the special gravity.

2.2.4. Ultrasonic Waves

Another way to define the density of a fluid is by using ultrasonic waves. Figure 2.9 found in [33] shows a very simple way to measure the density of a sample using ultrasonic waves: An ultrasonic wave is generated on one side of a sample and then is transmitted through the sample. When it reaches the other side of the sample the time between the transmission and the reception of the signal is then known. From those facts the density of the sample can be calculated. The results obtained from this technique were about 3-10% accurate.

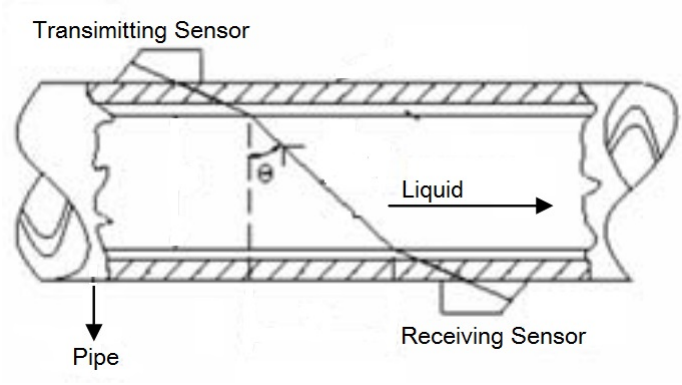

Figure 2.9: Typical hydrometer in measurement setup

Another technique is described in [27]: here the ultrasonic waves are reflected by a wire inside the sample. Here the density is calculated by the pressure experienced by a sensor that receives the reflected ultrasonic wave from the wire. The technique described in that paper achieves 1% accuracy according to the writers.

2.2.5. Radiation

Another way to measure the density of a fluid is by using particle radiation. [31] describe a set-up of a gamma-ray densitometer. A source of gamma ray is pointed towards the volume under measurement. A detector working in counting mode is placed next to the detector. The sensor and the source are separated by a radiation shielding, in order to avoid counting particles coming right from the source. Due to the Compton scattering, some gamma particles are reflected back to the sensor. An empirical relation of the following form can be used to relate the count rate of the sensor and the density of the sample:

$$I(\rho) = K_1 \rho \exp^{-C\rho} + K_2 \rho \exp^{-B\rho}$$

where: K_1, K_2, C, B are constants dependent on the instrument and can be defined through calibration. This technique is highly sophisticated and is best suited for laboratory or large scale industry.

It has become clear that in order to measure the salinity of a sample using its specific gravity a measurement of its density is the most crucial part. Another important factor is the composure of the sample, since all the techniques mentioned are not specific to NaCl or any other solid dissolved in water.

2.3. Titration

Titration is a technique that found wide usage in the past, before conductivity measurements were available.

The method relies on the interaction between bases, acids and indicators. Depending on the compound needed to be identified an appropriate titrant and indicator are used. A titrant is a sample of well known concentration of its compound. A known volume of the substance under examination is contained in an erlenmeyer. A small quantity of an indicator is then added to the sample under examination. After that, with the use of a burette containing a well specified amount of the titrant, the titrant is drop-by-drop added to the sample until the endpoint of the titration, when the colour of the sample changes, due to the interaction of ions of the titrant and the indicator.

In case of NaCl according to [4] and [16] titrant often used is silver nitrate ($AgNO_3$) and the indicator is potassium chromate (K_2CrO_4).

The chemical reactions taking place with the addition of the titrant are 2.

Initially the titrant Ag^+ ions interact with the sample's Cl^- ions with the following reaction:

$$Ag^+_{(aq)} + Cl^-_{(aq)} \rightarrow AgCl_{(s)}$$

The endpoint of the titration occurs once al the Cl^- are precipitated. After that the Ag^+ react with the $CrO^{2-}{}_4$ with the following reaction:

$$2Ag^+_{(aq)} + CrO^{2-}_{4(aq)} \rightarrow Ag_2CrO_{4(s)}$$

The change of colour noticed in the sample that signals the endpoint of the titration is due to the above mentioned reaction.

Titration measures the chlorinity of the sample. Using the empirical formula connecting salinity to chlorinity discussed on par 2.2.1 salinity can be calculated.

2.3.1. Ion Selective Electrodes

In order to proceed further into potentiometric titration it is important to analyse and explain the working principle of an ion-selective electrode.

According to [15] an ion-selective material includes any substance that alters physical or chemical properties in a quantitative, reversible way when it interacts with an ion. In addition it should usually display selective properties to a specific ionic species.

An Ag/AgCl electrode is a glass electrode. Figure 2.10 shows a standard glass Ag/AgCl electrode. Part of this electrode is a pH-sensitive glass membrane bulb which encloses a HCl buffer solution. Inside the bulb there is a internal reference wire out of Ag, covered by an AgCl layer. A second reference electrode made out of Ag, covered by an AgCl coating as well completes the circuit. This last electrode contacts the solution under measurement through a porous wick [42].

The measured quantity is the voltage difference between the two electrodes. The measurement electrode has a pH-sensitive glass membrane. When the electrode is immersed into water H^+ ions are allowed to penetrate the boundary area of the glass membrane. This causes a charge separation in the solution. The same phenomenon takes place inside the electrode, where the H^+ ions of the reference solution also penetrate the boundary of the membrane. In this case the ion concentration is known. The difference of H^+ on the two sides of the glass creates the potential difference measured by the Ag/AgCl electrode.

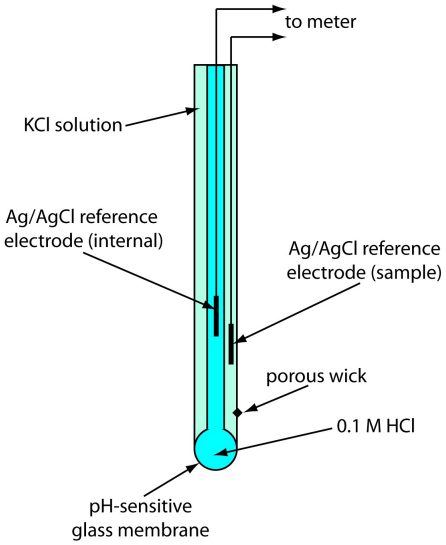

Figure 2.10: Ag/AgCl electrode

According to [10] the potential difference measured by the ISE follows the Nernst equation:

$$E = E_0 - 2.303\frac{RT}{nF}log(C + C_0)$$

where:

E is the measured potential (mV) between the ion selective and the reference electrode,

E_0 is the measured potential (mV) between the ion selective and the reference electrode at a C = 1 concentration,

R is the universal gas constant,

T is the temperature in Kelvin,

F is the Faraday constant,

n is the electrical charge of the ion,

C is the unknown concentration and

C_0 is the detection limit.

The detection limit of such a sensor is given by the plot of Voltage(log(C)).

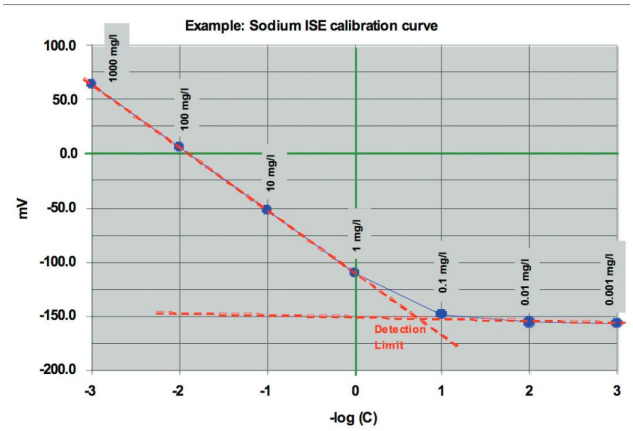

Figure 2.11: Ag/AgCl electrode

Figure 2.11 shows the calibration curve of an ISE, using samples of different Na^+. As it can be seen after 0.1mg/L the voltage becomes almost stable. This is hence the measurement limit of the particular ISE.

From the reaction of salt into water it is found out that Na^+ and Cl^- have a 1-1 relation meaning that there is an equal amount of both compounds.

There are also Cl^-. For example there is [1], that measures chlorinity in the scale between 10 and 20,000 mg/L and has an accuracy of 10% in the whole scale.

Measurements of salinity using such electrodes can be accurate, but requires frequent calibration and some level of expertise from the user to achieve accuracy. Furthermore those electrodes can be expensive as the [1]

2.3.2. Potentiometric Titration

Apart from traditional titration there is also potentiometric titration that offers higher accuracy. In this method the endpoint is detected potentiometrically using an Ag/AgCl electrode.

During potentiometric titration the titrant's volume added to the studied sample is plotted against the measured potential. The end-point of the titration is the point where the slope of the titration curve is maximum. An example of titration plot can be seen on Figure 2.12

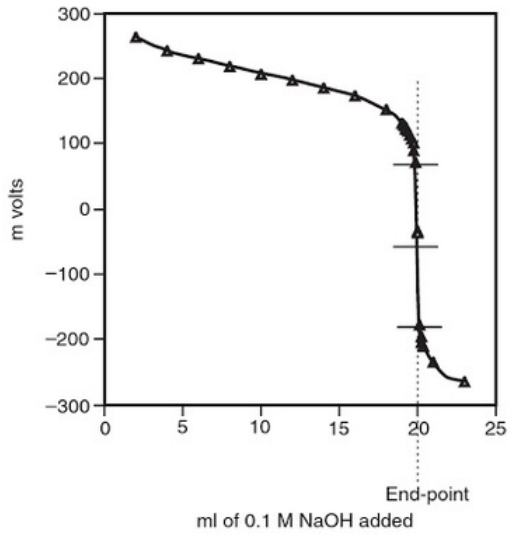

Figure 2.12: Titration of 20mmoles of aspirin with 0.1M NaOH

[42] and [21] informs that potentiometric titration is superior to the standard titration in every aspect:

it can be used in coloured samples,

it can detect the end-point more accurately when the change of colour is not that obvious,

it is more precise and

is faster.

Nevertheless titration is a technique that requires indicators, titrants, Ag/AgCl electrodes accompanied with the proper machinery to do the read-out and expertise on the side of the user.

Apart from potentiometric titration [21] suggests several other variations of titration such as:

UV-Vis Spectrophotometric Methods

NMR-titration

Liquid chromatography

2.4. Impedance Spectroscopy

Impedance is a measure of the ability of a circuit to resist the flow of altering current [20]. Impedance is in general a complex parameter. It can be used to define the permittivity and the capacitance of the electrochemical cell.

In order to measure the components of this complex number a small amplitude AC voltage is applied on the studied electrochemical cell as shown in Figure 2.13 [35] that and then its response is observed. There several ways to present the data of such an analysis: in the past Lissajous figures where used and more recent Nyquist and Bode plots are used.

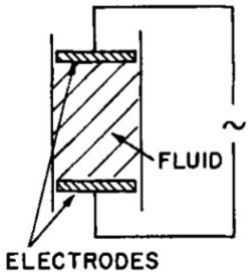

Figure 2.13: Impedance Measurement

As it is already noted impedance analysis is a complicated process. In order to process the data collected several models are proposed. Those models are equivalent circuits, used to describe explain the data collected. The most common equivalent circuit is the Randles circuit [7], shown in figure 2.14

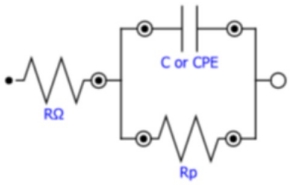

Figure 2.14: The typical Randles circuit

where:

R_Ω is the solution resistance experienced by the two electrodes,

R_P is the resistance due to the chemical reactions taking place on the contact surface of the electrodes and the sample and

C_{SP} is the double layer capacitance.

In order to describe all the phenomena taking place during an impedance analysis and in order to better explain the data there are several different equivalent circuits available. For example, Figure 2.15 shows an equivalent circuit used in order to study the corrosion of low carbon steel in NaCl solution [7].

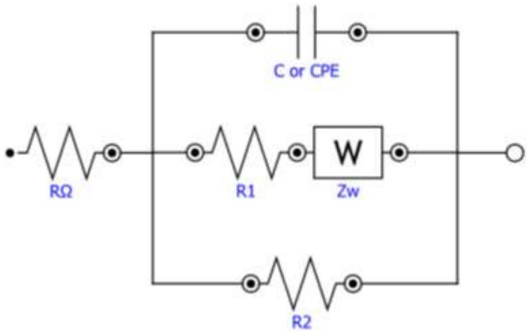

Figure 2.15: Equivalent circuit

where:

R_Ω is the solution resistance experienced by the two electrodes,

R_1, R_2 are the resistance values due to the chemical reactions taking place on the contact surface of the anode and the cathode and the sample respectively,

C_{SP} is the double layer capacitance and

Z_w is the Warburg impedance used to simulate the mass-transport effects (for further information [3]).

There can be even more complex equivalent circuit in order to capture more details of the phenomenon under study.

Impedance spectroscopy is done with the use of impedance analysers, that can scan the spectrum from a few Hz up to around 100MHz. This kind of equipment is expensive lab equipment that requires expertise from the user and frequent calibration.

2.4.1. Double layer Effect

The double layer effect occurs when a pair of electrodes is injected in an electrolyte and there is a DC difference of potential applied between them [36]. On the interface of the electrode and the electrolyte negatively charged ions are attracted by the "holes" of the positively charged electrode and get absorbed by the electrode. Another, wider and looser layer is formed around the first layer because of electrostatic forces (Figure 2.16). The opposite procedure happens on the other electrode.

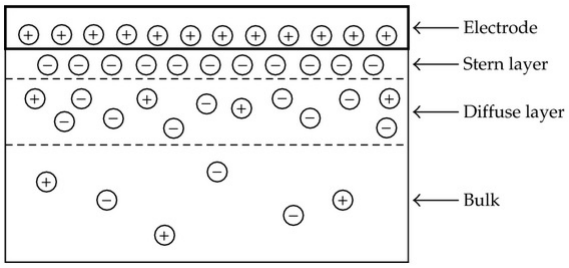

Figure 2.16: Equivalent circuit

The double layer effect is a non-Faradaic process, because the current that occurs in the sample is only due to the rearrangement of the ions inside it.

Figure 2.17 (taken from [36]) shows an equivalent circuit used to simplify the double layer effect.

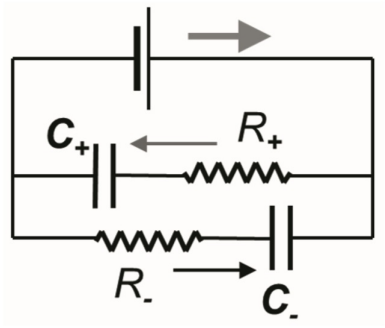

Figure 2.17: Equivalent circuit for the double layer effect

where:

V_{AC} is the voltage applied between the two electrodes

R_- and R_+ are the resistances of the medium to the ionic movement and

C_- and C_+ are the valu anions, respectively

From this circuit it can be derived that:

$$i = \frac{V_{AC}}{R_+} e^{\frac{-t}{R_+ C_+}} + \frac{V_{AC}}{R_-} e^{\frac{-t}{R_- C_-}}$$

Figure 2.18 shows the fit between experimental data and the previous relationship:

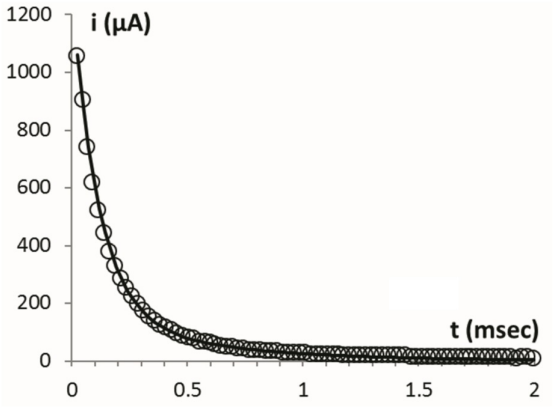

Figure 2.18: Plot of experimental data and theoretical model

From the previous relationship t=0

$$i = V_{AC}(\frac{1}{R_+} + \frac{1}{R_-})$$

From the last relationship it is suggested that the magnitude of the current inside the sample, for a given voltage, contains information about the concentration of the dissolved ions and therefore it can be correlated with the conductivity of the samples.

2.4.2. Electrical Conductivity

The electrical conductivity of a sample is related to the R_Ω from Randles circuit. By measuring the electrical conductivity of a sample it is possible to determine the total dissolved solids of the sample [17].

During a conductivity measurement, AC voltage has to be applied in order to avoid the electrolysis effect taking place in the sample. The Ac frequency has to be high enough in order to avoid the double-layer effect taking place since it distorts the measurement.

Water is an insulator, because its molecules are of neutral charge, meaning there are no electric carriers and thus no current can occur if voltage is applied between two probes injected to it. The picture changes totally when solids, like NaCl crystals, are added to water. When solids are mixed with water they dissolve in ions (in Na+ and Cl- in case of table salt).

Conductivity is measured by a probe, which applies voltage between two electrodes. The ionic current is used to measure the resistance of the water. By inverting the found resistance the conductance can be found.

Conductance is not a sample's quality as it is related to the probe used for measurement. Conductivity, which is a samples quality can be calculated by the formula:

$$\sigma = Gc$$

where:

σ is the conductivity

G is the inverse of resistance, known as conductance

c is the cell constant.

The value of cell constant depends on the dimensions of the probe and its shape. It can be calculated theoretically or it can be found experimentally using reference samples of known conductivity.

Depending on the desired measurement range of conductivity the cell constant must be chosen accordingly. Table 2.1 taken from [12] indicates the cell constant values for optimal conductivity measurement:

Cell Constant (cm^{-1})	Optimal Conductivity Range ($\mu S/cm$)
0.1	0.5 to 400
1.0	10 to 2000
10.0	1000 to 200,000

Table 2.1: Cell constant and conductivity optimal range

[8, 14, 17] suggest that conductivity is heavily influenced by temperature. [17] proves that the Sorensen and Glass equation:

$$EC_t = EC_{25}\left[1 + a(t-25)\right]$$

where:

EC_t is electrical conductivity at temperature t (^{o}C),

EC_{25} is electrical conductivity at 25^{o}C and

$\alpha\left({}^oC^{-1}\right)$ is a temperature compensation factor.

A common value according to [17], given to α is 0.02 or 2% increase of EC for each 1 ^{o}C increase of temperature above 25^{o}C. In the same work the value of α is measured experimentally and it was found to be equal to $0.0185\,{}^oC^{-1}$.

There are several different instruments that using the principals described before can measure the conductivity of a sample.

The most common instrument is the one with two electrodes at a certain distance. An altering voltage is applied between the two electrodes and by measuring the voltage drop of between them because of the sample, the witnessed resistance can be measured. By knowing the cell constant of the probe that can be analytically calculated the conductivity of the sample can be found. Commercially available sensors [2] can be found for around 20 € and they have a measurement range 0-9990μS/cm with resolution of 1μS/cm between 0-999μS/cm and 10μS/cm for the rest of the spectrum and an accuracy of 2%. They also compensate for temperature differences. In order to make sure that they function properly they need calibration, by using a reference fluid every now and then. The use of the equipment is straight-forward and it does not require any expertise.

There are other probes using 4 electrodes in order to measure the conductivity with higher accuracy over a greater spectrum of values. Figure 2.19 shows the arrangement of electrodes in a 4-electrode probe, the signal is applied between two outer electrodes and the measurement is made by the two inner electrodes. In this setup the measurement electrodes draw very little current and because of that charge transfer effects are not present at the metal-liquid interface. this gives the 4-electrode sensor a much wider range where the value of the cell constant is the same. The range for such sensors can be between 0 and 14,000,000μS/cm [14].

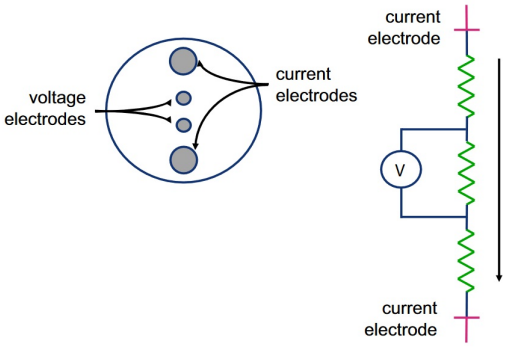

Figure 2.19: Usual 4-electrode probe layout

[14] argues that the measurement is affected also by the distance of the walls of the beaker, as well as the material of it as seen in Figure 2.20

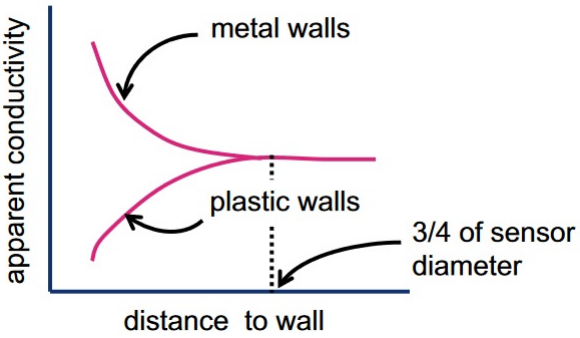

Figure 2.20: For typical sensors, wall affects disappear when the clearance between the sensor and wall is 1 – 1 ½ in (25 – 37 mm).

Another kind of instrument used to measure conductivity can by an inductive or toroidal sensor according to [14] (Figure 2.21): "An inductive sensor consists of two wire-wound metal toroids encased in a corrosion-resistant plastic body. One toroid is the drive coil, the other is the receive coil. The sensor is immersed in the conductive liquid. The analyser applies an alternating voltage to the drive coil, which induces a voltage in the liquid surrounding the coil. The voltage causes an ionic current to flow proportion- al to the conductance of the liquid. The ionic current induces an electronic current in the receive coil, which the analyzer measures. The induced current is directly proportional to the conductance of the solution."

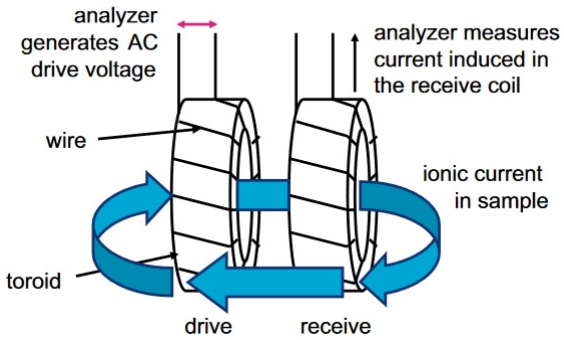

Figure 2.21: Usual 4-electrode probe layout

The instrument needs to be fully immersed in the liquid, but the toroids do not come in direct contact with the liquid. They can be used to detect salinity values greater than 15μS/cm and they are usually used in industry.

In [28] calculate the cell constant for planar interdigitated electrodes used for conductivity sensors. Due to the lack of any regular symmetry (Figure 2.22) the cell-constant is hard to be calculated analytically, but this paper, by doing some complex calculation offer an analytical expression for the cell constant. 3 The key advantage of such probe is the very low cost to manufacture as well as the fact that the probe can be part of the PCB used for the electronics of the sensor, makes it easy and fast to assemble.

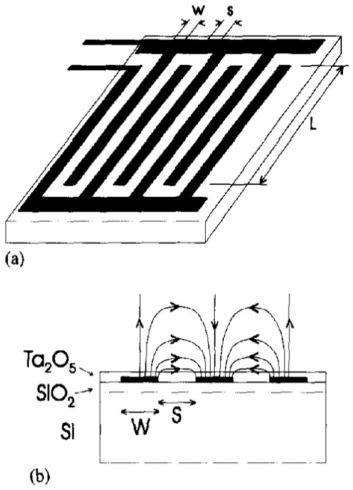

Figure 2.22: (a) The interdigitated electrode
(b) Electric field lines

2.4.3. Microwave Spectroscopy

Microwave spectroscopy is the study of the interaction of matter and electromagnetic radiation in the microwave region of the spectrum (approx. 300MHz-300GHz). According to [24] any substance interacts with electromagnetic waves in a unique way. This interaction can be used to identify qualities of the material. During this interaction the permittivity of the material changes, manifesting itself as frequency shift, reflection or attenuation of the signal. By measuring the transmitted (S_{21}) and reflected (S_{11}) microwave energy information can be acquired on the composition of the sample.

[30] designed and tested a novel microwave sensor. They used a cavity resonator sensor, that measured the reflected energy S_{11}. In that work they reported two frequency areas that could be used in order to determine the salinity of their samples. Their results are shown in Figure 2.23.

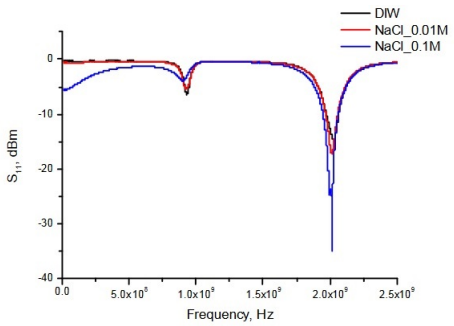

Figure 2.23: NaCl peaks detected by resonant cavity sensor at low microwave frequencies.

The first peak is around 800MHz and the second peak is around 1.8GHz. This work used only three aqueous samples: di-onized water and two NaCl solutions with 0.01M and 0.01M. [23] made a more thorough measurement of the peak detected at 1.8GHz, using more samples with different salinities. Figure 20 shows their results:

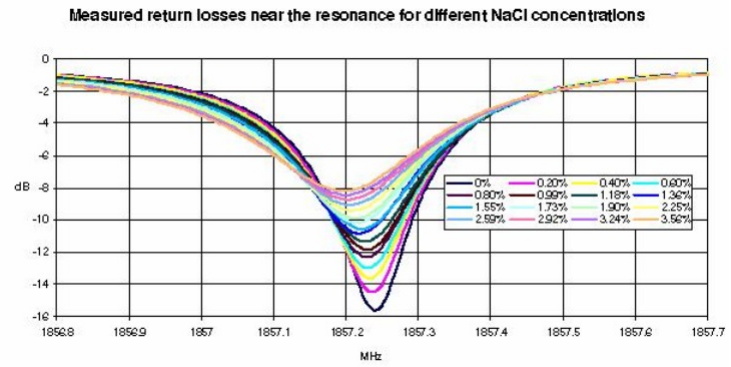

Figure 2.24: NaCl peaks detected by resonant cavity sensor at low microwave frequencies(Detailed).

As it can be noticed in this graph the frequency of maximum return loss (reflected energy or S_{11}) shifts with the change of salinity, but the writers of the paper suggest that this shift is negligible. They even offer a calibration curve of their sensor, shown in Figure 2.25.

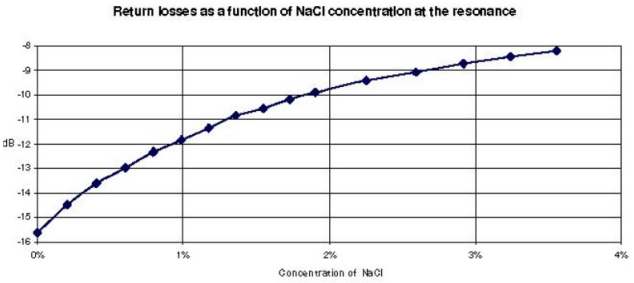

Figure 2.25: Microwave sensor calibration curve

Overall, microwave spectroscopy can be used to implement in-situ, real-time, non-destructive and accurate concentration measurements of specific solids, such as NaCl, KCl, etc. The short-coming of the microwave spectroscopy is that at the moment requires some level expertise in making the measurements and the fact that, as most of the previous techniques it is influenced by factors such as temperature.

2.5. Raman Spectroscopy

Raman spectroscopy is an accurate and highly sophisticated, in terms of instruments used, technique to detect and quantify various compounds in samples.

A monochromatic light source (laser) is shinned on the sample and all the scattered light gets detected. The majority of the light undergoes the Rayleigh scatter, keeping the same wavelength as that of the source, there is a very small part of light that after the scatter has its wavelength and hence its frequency shifted. The reason why this happens is because of the interaction between the electromagnetic waves and the vibrational energy levels of the molecules of the sample. Plotting the intensity versus the frequency results in the Raman spectrum.

Each molecule or element has each own characteristic Raman spectrum and in this way it is possible to identify each compound in the sample. Usually Raman spectroscopy is performed in visible wavelengths. At those wavelengths water in gas or liquid form is almost invisible to that light and this makes Raman spectroscopy ideal for the study of aqueous solutions. In order to estimate the concentration of a compound the shift of the frequency is used[32].

[9] argues that a pure H_2O sample has 3 peaks at 3223cm$_{-1}$, 3433cm$_{-1}$ and 3617cm$_{-1}$. According to the writers there is a linear relationship between the shift of the the peak at 3223cm$_{-1}$ and the NaCl concentration. This relationship is described by the linear equation:

$$\Delta v_1 = 3222.8 - 1.69sal$$

where:

sal is the salinity in % mass units and

$\Delta\nu_1$ is the relative wavenumber

Figure 2.26 is the plot of intensity of the Raman spectrum vs. the relative wave number:

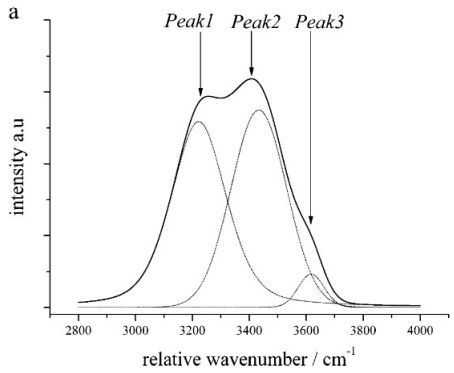

Figure 2.26: Deconvolution of Raman Spectrum of pure water

[44] provides with a detailed analysis of the relationship between the temperature, salinity and the shape of the Raman spectrum. Figure 2.27 is again a plot of intensity of the Raman spectrum vs. the relative wave number, but for 5 different NaCl solutions:

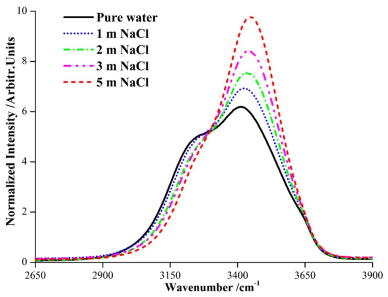

Figure 2.27: Raman Spectrum of different NaCl solutions

From the same source plots for different solutions are shown on Figure 2.28.

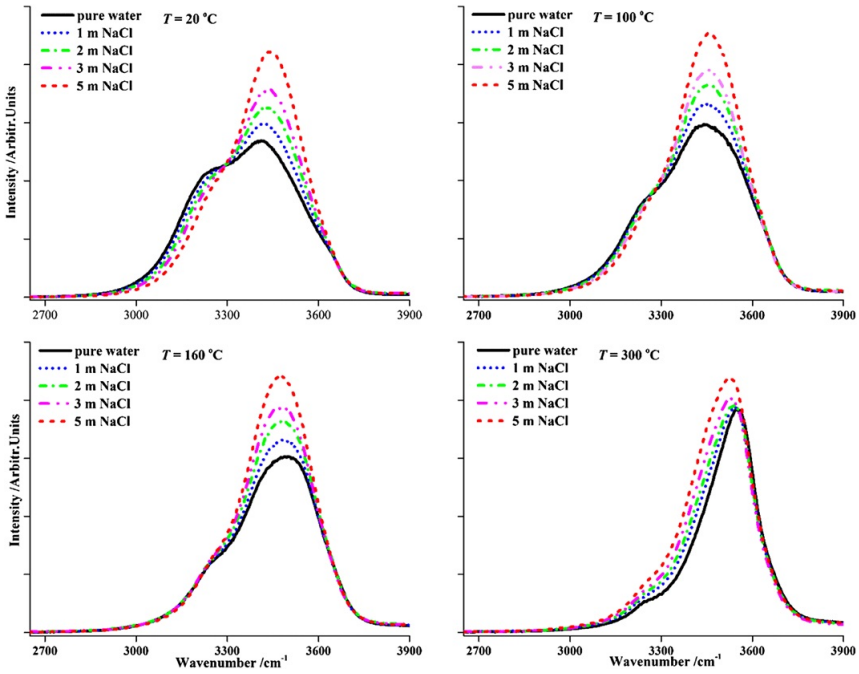

Figure 2.28: Raman Spectrum of different NaCl solutions at different temperatures

Raman spectroscopy can identify and quantify various different components with high accuracy. At the moment, mostly due to the need of the laser, it is strictly a lab-technique, that requires a high level of expertise.

2.6. Discussion and conclusions on the methods

The previous chapter was dedicated on the description of the physical principles, ways of measurement and evaluation of techniques available to measure the salinity of an aqueous sample. On this chapter there will be a brief and solid comparison between those techniques, based on the main criteria set in the beginning of the project:

Accuracy

Resolution

Cost

Portability

Ease of use and maintenance

Table 2.2 summarizes the how each reviewed method meets the criteria set above. The method that fits all the criteria in the best way is the electrical conductivity measurement, using an interdigitated probe. This measurement is basically an impedance spectroscopy technique, where the capacitance is ignored in Randles circuit. Using a high frequency, the double layer effect is minized and so does the capacitance because of it, so it can actually be neglected.

Method	Accuracy	Cost	Portability	Resolution	Ease of use
Optical(Refractometer)	- - -	$	+++	- - -	++
Specific Gravity (Hydrometer)	- - -	$	+++	- - -	++
Specific Gravity (Ultrasonic Waves)	+	?	- - -	- -	+
Specific Gravity (Radiation)	++	$$$	- - -	++	- - -
Titration	++	-	$$$	-	- -
Potentiometric Titration	+++	$$$	- - -	+	- - -
Ion Selective electrodes	++	$	+++	++	+
Double layer Effect	?	?	?	?	?
Electrical Conductivity(2-electrode probe)	++	$	+++	+++	++
Electrical Conductivity(4-electrode probe)	++	$$	+++	+++	++
Electrical Conductivity(Toroid probe)	+++	$$$	+++	+++	++
Electrical Conductivity(Interdigitated probe)	++	$	+++	+++	++
Microwave Spectroscopy	+++	$$$	- - -	+++	- - -
Raman Spectroscopy	+++	$$$	- - -	+++	- - -

Table 2.2: Salinity measurement methods comparison table

3

Impedance Spectroscopy: Proof of Concept

3.1. Introduction

As it was pointed out in the end of chapter 2 the method chosen in order to measure the conductivity of water is the impedance spectroscopy, using interdigitated probes. The reason behind this choice is the fact that it is one of the most reliable, widely-used techniques, that also covers the accuracy, range and portability requirements, while the cost can remain low.

This chapter describes a set of measurements that was made in order to verify the assumptions and expectations from the impedance spectroscopy. At the time of the measurements the means available were a coaxial probe and an impedance analyser.

In order to determine that using impedance analysis it is possible to observe discrete levels of conductivity for water samples with different NaCl concentration and hence different conductivity, 11 samples of different NaCl concentration were made using de-mineralized water and NaCl crystals. Salt was weighted in a precision scale in order to create NaCl concentrations of high precision. The experiment was conducted in room temperature (23oC). The solutions had the following concentrations: 0%, 0.035%, 0.07%, 0.105%, 0.14%, 0.175%, 0.21%, 0.245%, 0.28%, 0.315% and 0.35%. Finally another solution of 1% NaCl was built in order to examine the electrical conductivity at nearly sea level concentrations. The choice to make those samples was made in order to determine the resolution of the method.

The measurements made refer to the equivalent parallel conductance and equivalent parallel capacitance. For those measurements the option CP-G of the **Agilent 4294A Precision Impedance Analyser** was used. The bandwidth of measurement was 350 Hz up to 110 MHz and the resolution used was 201 frequency points. A Matlab script (A.1) based on Johan Vogel's script was used in order to retrieve the data from the impedance analyser. The amplitude of the applied signal was 500mVolts.

3.2. Measurements

3.2.1. First set of measuremetns

The results obtained from those measurements are shown in Figures 3.1, 3.2

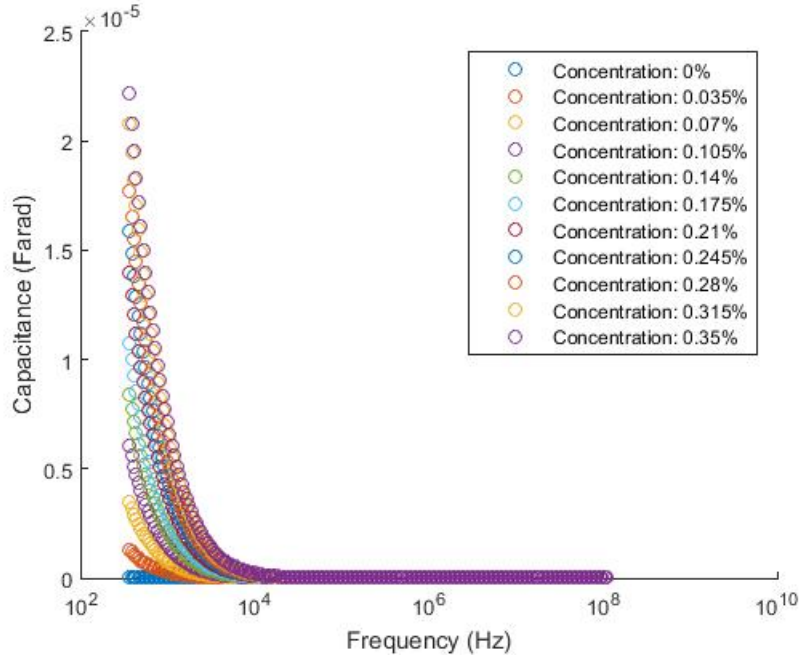

Figure 3.1: Capacitance vs. Frequency

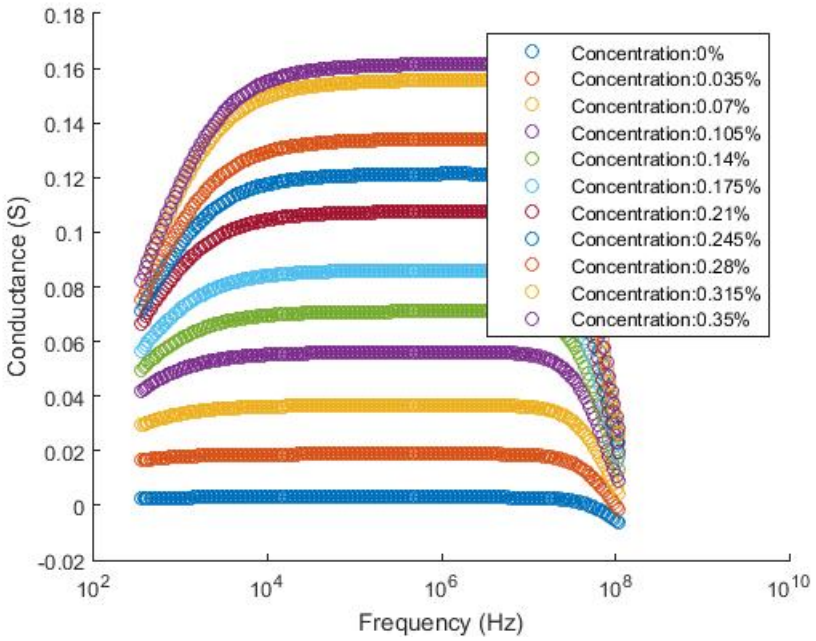

Figure 3.2: Conductance vs. Frequency

3.2.2. Discussion on results and motivation for further investigation

As it can be seen in Figure 3.1, the capacitance of the sample is affected by its conductivity , but the curves obtained are far more difficult to be used compared to those from 3.2. Furthermore, there is significant overlapping of the curves for different conductivities.

The spectrum above 1 MHz is of no interest in this case, because for higher values the measurement stays the same. For even higher values the outcome is a reduced value of conductance. This is because of the fact that the conductance is the result of the mobility of ions in the water, but by applying a signal of very high frequency, causes the ions to practically not move hence reducing the conductance.

Another interesting feature of the results is that when a signal of low frequency is applied, measured conductance reduces. This phenomenon becomes really clear on high-concentration solutions. The reason for that is the double-layer effect. When the frequency of the signal is low, ions accumulate around the corresponding electrode, reducing the electric field in the solution. As a result ions in the solution are subjected to a smaller field and so their coordinated movement is reduced, leading to a smaller current and hence conductance.

3.2.3. Second set of Measurements

In this new set of measurements only the conductance is of interest as stated above.

Figure 3.3 shows the outcome of the results from 350 Hz up to 1 MHz:

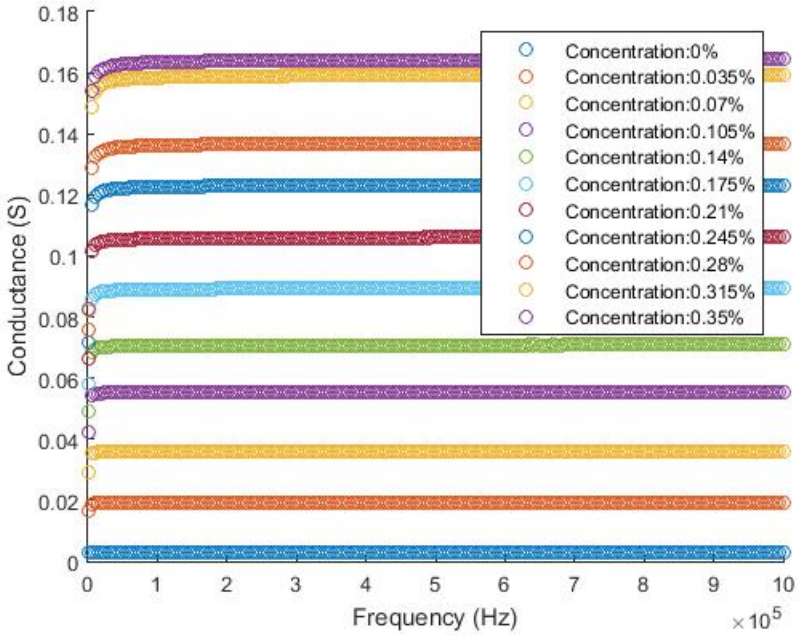

Figure 3.3: Conductance vs. Frequency

3.3. Calculation and experimental measurement of cell constant of the probe

In order to compare the readings of the individual sensors it is necessary to convert conductance to conductivity, since the latter is the liquids characteristic quantity.

The relation between conductance and conductivity is:

$$conductivity = conductance * cell\ constant$$

where:

conductivity is the quality of the medium, usually measured in μS/cm or mS/cm,

conductance is measured in μS or mS,

the cell constant of the probe is usually given in cm^{-1}.

The cell constant can be calculated analytically or measured experimentally.

3.3.1. Experimental measurement of cell constant

In order to define the cell constant experimentally, solutions of known conductivity are subjected to measurement, using the probe under investigation. The cell constant is then calculated using the formula:

$$cell\ constant = \frac{conductivity}{conductance}$$

To define the cell constant experimentally two samples with standardised conductivity were used:

- 1.413mS/cm
- 12.880mS/cm

To measure the cell constant results for frequencies above 100 kHz were taken into account, since there is an important impact of the double-layer effect for lower frequencies.

The results obtained by the measurements are shown on Table 3.1:

Conductivity (mS/cm)	Cell constant (cm^{-1})	Error
1.413	0.0422	0.0053
12.880	0.0391	0.118

Table 3.1: Cell constant measured with calibration fluids

3.3.2. Analtical calculation of coaxial probe cell constant

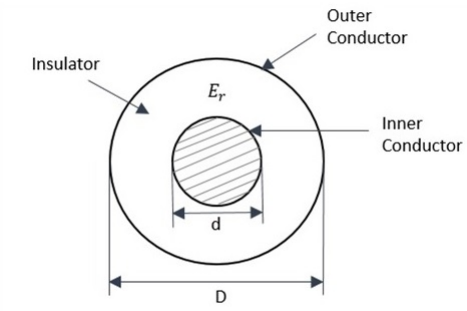

Figure 3.4: Coaxial symmetry

Assuming a linear charge distribution λ on the inner electrode of a coaxial cable as in Figure 3.4, Gauss law can be written as:

$$\oint_V \vec{E} d\vec{a} = \frac{\int dq}{\kappa\epsilon_0}$$

Due to the cylindrical symmetry of the problem and the fact that the direction of the field is radial the above equation can be written as:

$$\int_0^r E_r 2\pi l dr' = \frac{1}{\kappa\epsilon_0}\int_0^l \lambda dq \leftrightarrow$$

$$\vec{E_r} = \frac{\lambda}{2\pi\kappa\epsilon_0 r}\hat{r}$$

Knowing the electric field distribution inside the coaxial cable, the potential can be calculated by the formula:

$$V = \int_d^{r_\alpha} \vec{E} d\vec{r} = \frac{\lambda}{2\pi\kappa\epsilon_0}\int_d^{r_\alpha} \frac{dr}{r} = \frac{\lambda}{2\pi\kappa\epsilon_0} ln\frac{r_\alpha}{d}$$

So the potential difference between the inner and the outer electrode of the probe is

$$V = \frac{\lambda}{2\pi\kappa\epsilon_0} ln\frac{D}{d}$$

According to Ampere's law in the integral form:

$$I = \iint_S \vec{J} d\vec{S}$$

where:

$\vec{J} = \sigma \vec{E}$ is the current density and σ is the conductivity,

I is the current enclosed in the area surrounded by the area S and

$d\vec{S}$ is the vector area of an infinitesimal element of surface S.

So the equation becomes:

$$I = \int_S \sigma \vec{E} d\vec{S} = \int_0^{2\pi} \int_0^{l} \frac{\sigma \lambda r}{2\pi\kappa\epsilon_0 r} d\phi dz = \frac{\sigma\lambda}{\kappa\epsilon_0}$$

Conductance is the reciprocal of resistance, so b inverting Ohm's law the conductance is found to be:

$$G = \frac{1}{R} = \frac{I}{V} = \frac{\frac{\sigma\lambda l}{\kappa\epsilon_0}}{\frac{\lambda}{2\pi\kappa\epsilon_0} ln\frac{D}{d}}$$

Applying the previous relationship to:

$$\sigma = Gc \leftrightarrow$$

$$c = \frac{\sigma}{G} = \frac{ln\frac{D}{d}}{2\pi l}$$

where:

D is the inner diameter of the inner electrode,

d is the outer diameter of the inner electrode and

l is the length of the inner electrode.

This result is also supported from [34].
The dimensions of the used probe are:

Outside diameter	16mm
Inner diameter	5mm
Length	45mm

Table 3.2: Dimensions of measurement probe

The calculated value of the cell constant is 0.0411 cm^{-1}.

As it can be seen the theoretically calculated cell constant falls within the range of the experimentally measured cell constants in both cases.

After calculating the cell constant and using the conductance measurements it is easy to calculate the conductivity. For the calculations that follow the theoretical value is used.

3.3.3. Comparison between lab and commercially available equipment

In order to make a comparison with the standard equipment for the measurement of the conductivity (**Greisinger GMH 3431**), as well as the sensor that is under test, the previous solutions were measured.

The standardized and commercially available equipment uses a signal of 350 Hz and 20 mVolt amplitude.

Two plots were made in order to compare the results obtained with the lab equipment, working in two different frequencies with the ones obtained using the **Greisinger**.

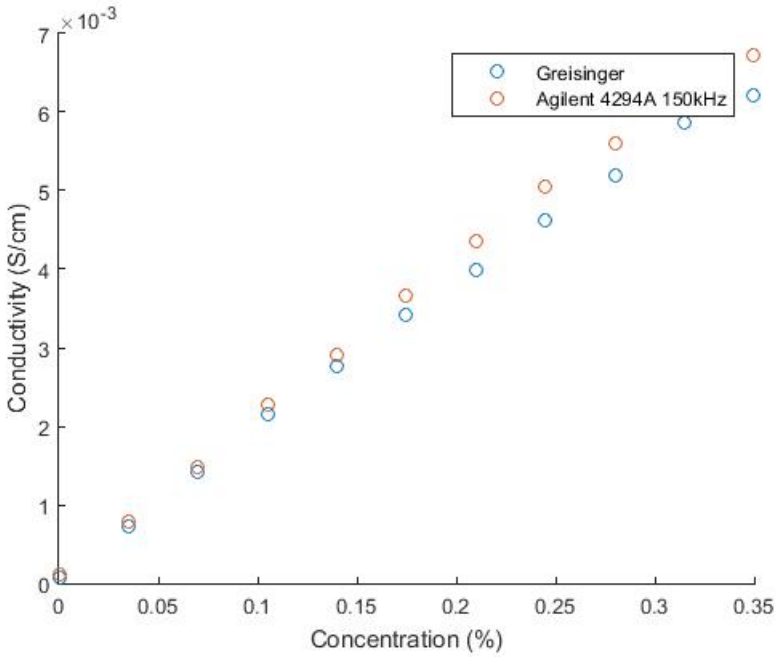

Figure 3.5: Conductivity as a function of concentration measured by Greisinger GMH 3431 and laboratory equipment using signal of 150kHz

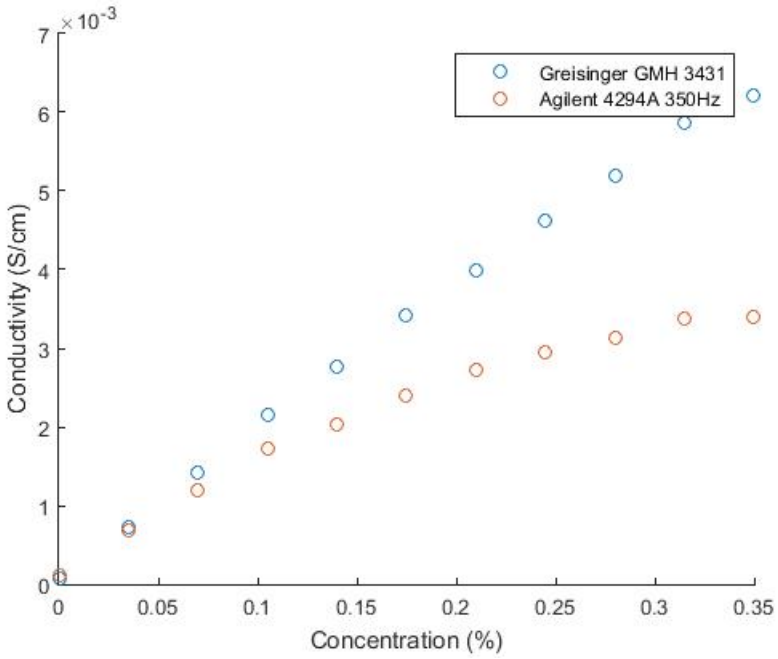

Figure 3.6: Conductivity as a function of concentration measured by Greisinger GMH 3431 and laboratory equipment using signal of 350Hz

3.4. Observations and conclusions

While measuring the capacitance and the conductance of the samples it was noticed that the capacitance observed was unaffected by the depth at which the probe was immersed into the solutions. On the other hand conductance was very much depended on the length of the probe immersed. So in order to make the measurements a standard depth was chosen at which not the whole probe was under water (this was taken

into account during the calculations of teh cell constant). Furthermore the more length of the probe was under the water the higher was the reading of the conductance by the **Agilent 4294A**.

The differences between the lab readings and the ones by the sensors can be explained by the fact that the sensors compensate for readings for temperatures different than 25^{o}C.

Another very important fact that can be seen in Figure 3.5 is the linearity of the readings from the **Agilent 4294A** at 150 kHz.

Figure 3.6 shows that for low frequencies, this probe is prone to the double layer effect. For this reason it is important to determine the frequency above which the readings become stable in the design of the final probe.

4

Design of probes

The following chapter describes the steps taken towards the design of the probe. All the parameters regarding the behaviour of the probe were investigated and are described in the following paragraphs.

4.1. Motivation

As it has been mentioned before, the cell constant is one of the most important factors in measuring conductivity. A well defined cell-constant renders the need of initial calibration of the sensor void.

One of the main issues in designing the probe was the need of consistency in the geometrical dimensions of the probe. Due to inaccuracies that occur during the manufacture of various components of the measurement probe there can be a noticeable difference in the value of the actual cell constant of each individual probe. This can translate into the need of a calibration process for each probe individually, which is not viable for a large scale production.

Another important issue needed to be taken into account while designing the probe is the ease of assembly, as this can have an important impact on the cost of the final system.

Finally it is of extreme importance to have a probe of well defined cell constant in order to maximize the accuracy and reliability of the measurement.

A very good candidate that meets most the above criteria are interdigitated-planar electrode probes. PCB probes can have practically identical dimensions (Eurocircuits offers 20μm accuracy), meaning that their cell constant will also have identical qualities. At the same time , since they are already part of the PCB, there is no time or effort spent in assembly. The only issue there is that due to the geometry of those probes there is no straightforward analytical possibility in calculating the cell constant of those probes.

[28] tackles this problem by suggesting an analytical expression in order to calculate approximately the cell constant of the probe. In their paper though there are many restrictions, some of them explicitly described, while others are implied. Those restrictions affect significantly the accuracy of the measured cell constant. Despite those drawbacks this work provides an excellent start point for the cause of the present thesis.

[43] designs, implements and calibrates such a sensor. In that work there is also an effort to derive an analytical expression to calculate the cell constant of the probe. The geometry in this case is simpler since there are two "fingers" of the same thickness at a known distance one next to the other.

4.2. Simulations

As it was discussed before [28] suggests that there are many limitations on their model as well as a great degree of uncertainty in their results. In order to have a more detailed view on the matter, as well as to be able to evaluate the accuracy of the predictions of their model COMSOL simulations were used.

There were 4 different models of probes that were created in order to choose the most suitable to choose from. Each model is subjected in a parametric sweep, where the parameter is the conductivity of the water sample that is in contact with the water. Conductivity variates between 0.0001μS/cm and 400μS/cm. The first model that was chosen is a simple configuration of two copper planes placed in parallel, with a water sample in between. This configuration has level symmetry and there is also an analytical expression to calculate the cell constant.

4.2.1. Parallel Plates

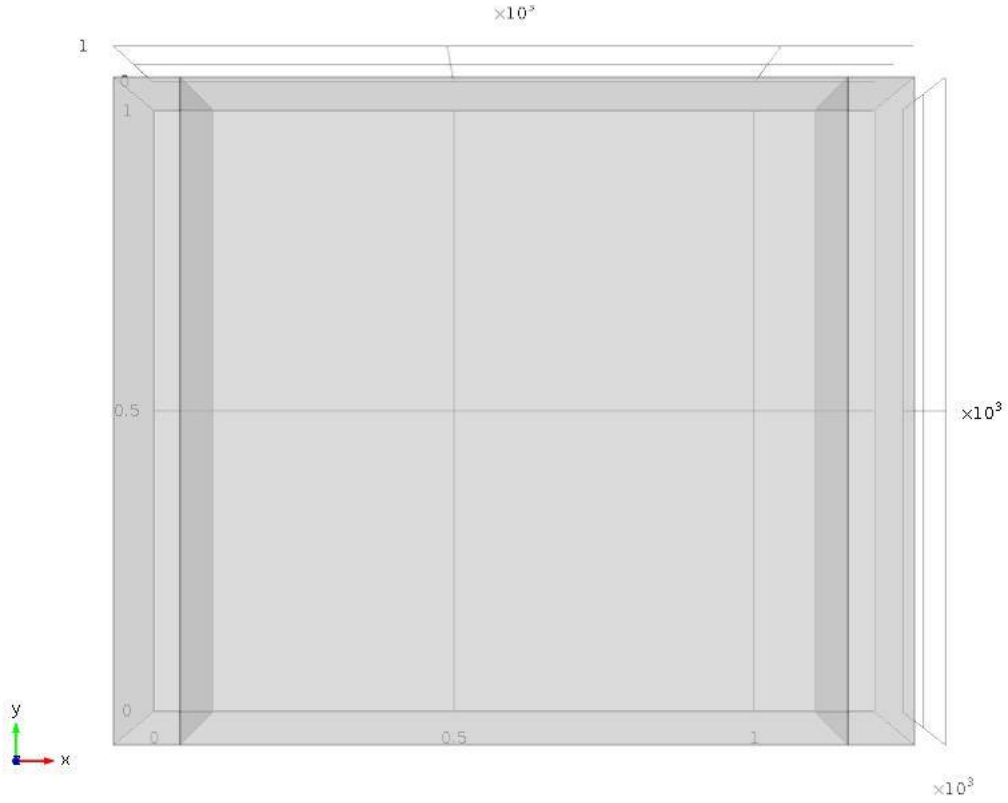

Figure 4.1: Parallel copper plates, with water in between

Figure 4.1 shows the model of two parallel square planes with a sample of water in between. Figure 4.2 shows the cell constant calculated from the simulation. The value is found to be 10 cm^{-1}.

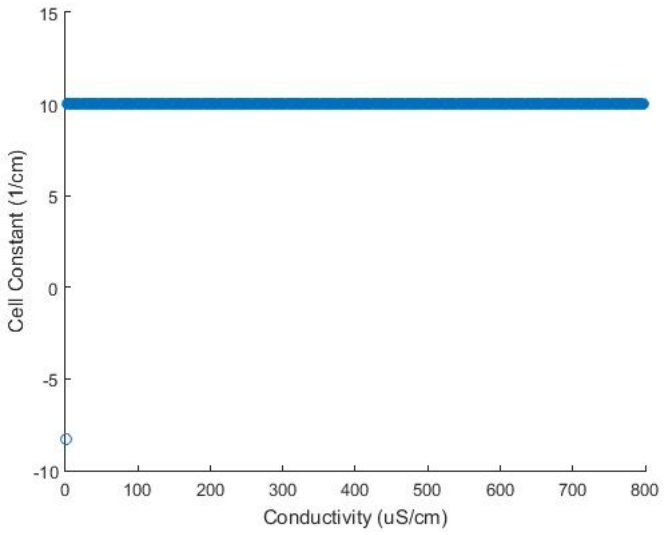

Figure 4.2: Cell constant plotted as a function of conductivity, in the case of two parallel plates containing a sample of water between them

The dimensions of this design are given in Table 4.1.

Dimension	Size (mm)
side	1
height	0.1
distance	1

Table 4.1: Dimensions of square parallel copper planes

The analytical formula calculating the cell constant for this configuration can be found at [28]. Their end result is that the cell constant is related to the capacitance between the parallel plates, with the following relationship:

$$cc = \frac{e_0 e_r}{C}$$

where:

ϵ_0 is the permittivity of vacuum,

ϵ_r is the relative permittivity of the medium,

C is the capacitance between the two plates.

Capacitance between two parallel planes is given by the following formula

$$C = \frac{e_0 e_r A}{d}$$

where:

A is the surface of the plates and

d is the distance between them.

Using this formula the result is again 10 cm^{-1}.

During the simulations an interesting fact was noticed: if the water sample is bigger than the size of the square plate, then the simulation results are different than the value calculated, because of the fringing field that is now applied on the larger sample of water that is available. Those fields are not taken into account into the theoretical calculations, since there it is assumed that all the field is contained between the two parallel plates. It is noticed that the cell constant drops as the water that is not covered by the water is increased. This is due to the fact that ions inside the water are experience the force of the fringing field and they move accordingly adding to the conductance caused by the ions that moved inside the homogeneous field between the two parallel plates. Despite this the cell constant appears to be really stable for different values of the conductivity of water, making this configuration really stable.

4.2.2. Two electrode strips

This simulation models and studies the work of [43]. The advantage of this configuration is its simplicity from a design point of vies. In this case, though, there is no analytical way to calculate the cell constant. There can only be either a direct measurement using calibration fluids or the results of a simulation. Figure 4.3 shows the configuration of this model. On top of the strips, there is a sample of water 5mm thick.

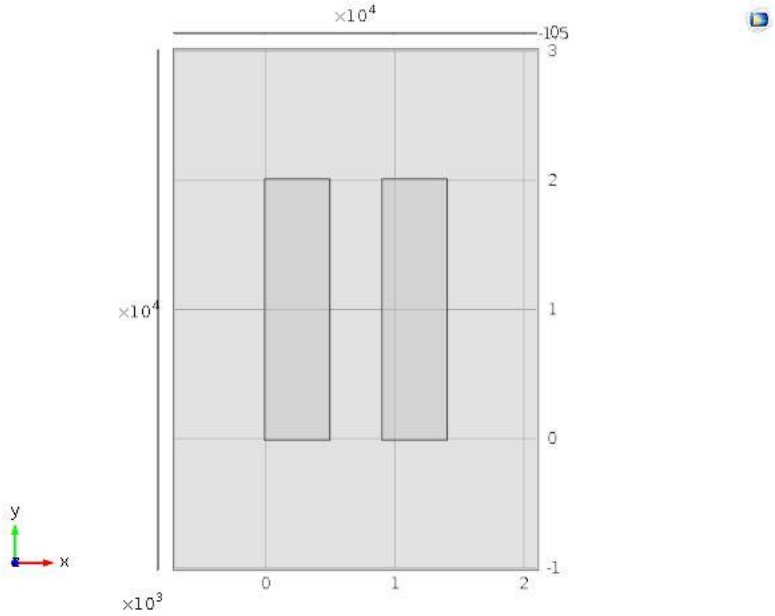

Figure 4.3: Electrode strips

Table 4.2 contains the dimensions of the electrodes, as well as the distance between them.

Dimension	Size (mm)
width	5
lenght	20
distance	4

Table 4.2: Dimensions of square parallel copper planes

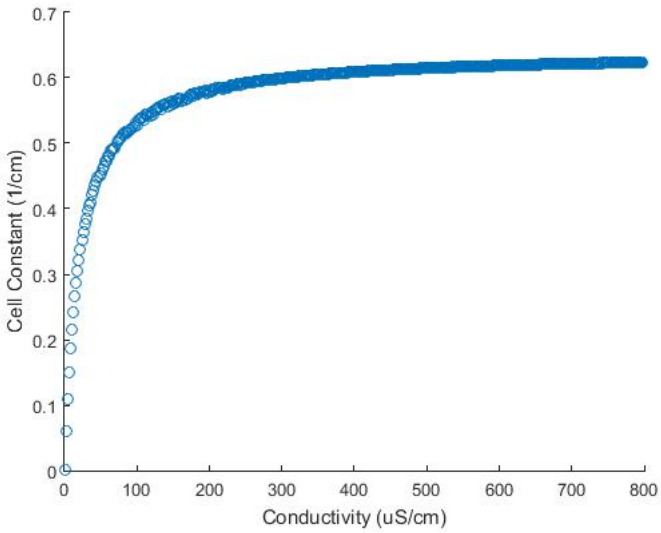

Figure 4.4: Cell constant plotted as a function of conductivity, in the case of two electrode strips immersed in water

Figure 4.4 is the outcome of the above described simulation. As it can be seen here the cell-constant is not a *constant* any more, unlike to the results obtained with the parallel plates. A more detailed analysis and explanation of this result follows in 4.2.5

4.2.3. Interdigitated Electrodes with 4 fingers

The next model was developed in order to study a configuration of electrodes similar to the probes suggested in [28]. As it was pointed out before this work has several limitations in the way results are presented and also to the restrictions posed to the physical dimensions of the electrodes.

The model presented here is such that it is actually placed outside of the implied restrictions of the paper. This choice was forced since the width of the electrodes as well as the spacing between them, suggested by the paper, was in the order of μm, which in turn is close to the manufacturers accuracy limits and would cause an uncertainty in the actual dimensions of each individual probe, creating an overhead of uncertainties and errors. An implied restriction is also that the length is about 2 orders of magnitude bigger than that of the width and this would lead to an unnecessarily bulky probe.

Table 4.3 contains the physical dimensions of the model and figure 4.5 shows the actual model.

Dimension	Size (μm)
width	650
lenght	950
Spacing on the x-axis	500
Spacing on the y-axis	1800

Table 4.3: Dimensions of square parallel copper planes

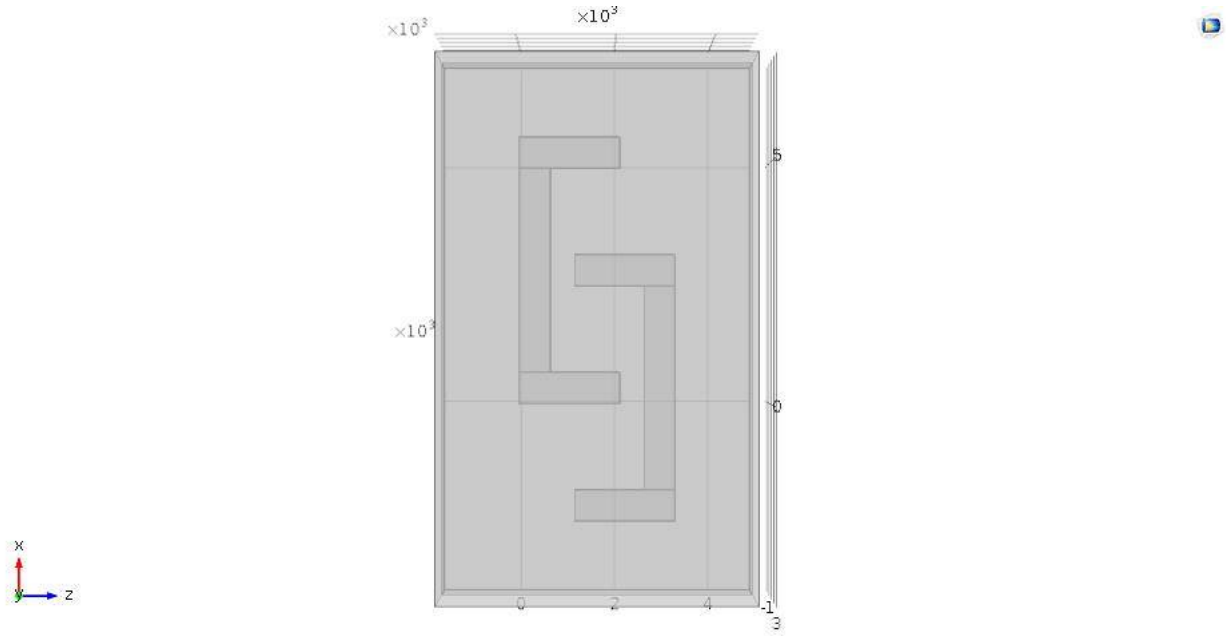

Figure 4.5: Interdigitated electrodes with 6 fingers

The results of the simulation are shown in figure 4.6.

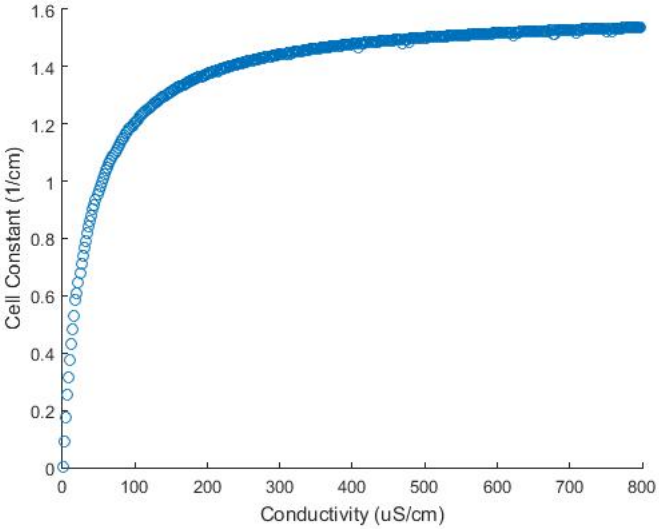

Figure 4.6: Cell constant plotted as a function of conductivity, with the probe immersed in the water

4.2.4. Interdigitated Electrodes with 6 fingers

In order to have a better understanding on the impact of the number of fingers to the cell constant and also to the stability of it, another model was created, with the same physical dimensions of table 4.3, but with 6 fingers this time.

The probe is shown in figure 4.7.

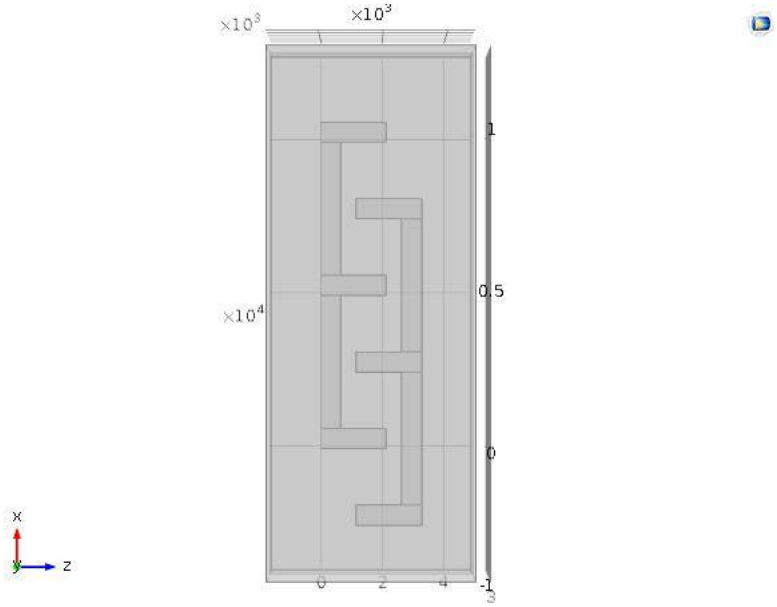

Figure 4.7: Interdigitated electrodes with 4 fingers

The results of the simulation are shown in figure 4.8.

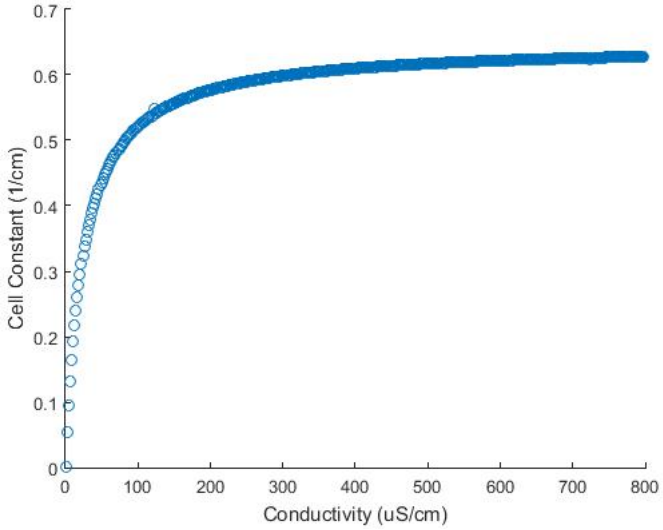

Figure 4.8: Cell constant plotted as a function of conductivity, with the probe immersed in the water

One profound observation is that the increase of the number of fingers decreases the value of the cell constant. Other than that the two designs seem to have similar qualities.

4.2.5. Cell constant curve of the Interdigitated planar electrodes

The observed behaviour of the cell constant curve cannot be found explicitly in the literature. There are many implementations based on the work of [28], that not even notice this behaviour. In [43] the curve is not even observed.

The only slight evidence that the phenomenon is observed can be found in Figure 2 [18]. That figure shows that there are significant errors between the measured conductivity and the actual one for low conductivity values (approximately 30%). This can be explained by the fact that there was a two point calibration of the sensor and two points are simply not enough to capture all the information of the curve of Figure 4.4.

At this point it is important to clear out what the cell constant is. The cell constant is defined as the ratio bellow:

$$cell\ constant = \frac{conductivity}{conductance}$$

where:

conductivity is a quality of the medium.

conductance is the outcome of the measurement made by any probe. It contains information both of the medium and the probe used.

In order to make it more clear, *conductivity* is the inverse of *resistivity* and *conductance* is the inverse of *resistance*.

So during the simulation the numerator is known (determined by the user) and the denominator is the quantity that is calculated.

As it was said before:

$$conductance = \frac{1}{resistance} = \frac{I}{V}$$

For the simulation, the voltage has a fixed value (during the simulation, various input voltages were used, but the results were always the same), so the only variable in order to calculate the cell constant is the current.

As mentioned before, the literature doesn't even presents this behaviour of the interdigitated probes, let alone explain it. Yet, as it can be seen by the simulation results, this behaviour is intrinsic to the interdigitated probes. An attempt to explain the observed results from the simulations follows:

When the conductivity is low, there are not many ions in the sample. This means that the current that can go through the medium cannot exceed a certain value (not enough charge to be mobilized). When the conductivity increases, so does the number of ions and now their number is adequate to form the current dictated by the voltage applied. In metals, generally the law of Ohm holds due to the abundance of electric charge offered by the valance electrons, but this is not true for a conductive solution: the moving charges in this case are ions and, for low conductivities there are not so many. So this means that the ratio between current and voltage of a conductive solution is not constant and so the medium is not Ohmic. For this reason the curve seems to become stable for higher values of conductivity.

Another fact that can help explain the behaviour of the cell constant is the shape of the electric field lines. In the case of the parallel plates, those lines are straight and contained between the planes (the fringing fields at the edges, are negligible). On the other hand the electric field of the interdigitated is basically a fringing field that is not easy to describe and the different ions, will feel different electric force, depending on their position regarding to the probe. Those fringing fields occur due to sharp edges of the probes and are the reason that an analytical calculation of the cell constant is not possible.

4.2.6. Probe design selection

The design that was finally picked in order to be implemented was the one with 4 fingers. The choice was made because of the fact that the cell constant value of this probe tends to go around 1,5 cm^{-1} which is a good value in order to measure a wide spectrum of conductivity values. This is the reason that it was chosen over the 6 finger design or any other multi-finger configuration.

The parallel plates have a construction overhead that can have an impact on the cost of the sensor and those are the reasons that they are not tried out.

Finally the probe with the two conductive strips has already been studied thoroughly and it seemed to be more interesting to study the selected design.

4.2.7. Probe design

Figure 4.9 shows the probe that was built for testing purposes. The dimensions of the probe are the ones found in Table 4.3

Figure 4.9: Test probe design

The results of Comsol simulations were used to determine the relationship between the cell constant and the conductance for this probe. Performing a rational fraction approximation of 1st degree for both numerator and denominator on the plot of the cell constant as a function of conductance for low conductivity values the results can be observed on 4.10.

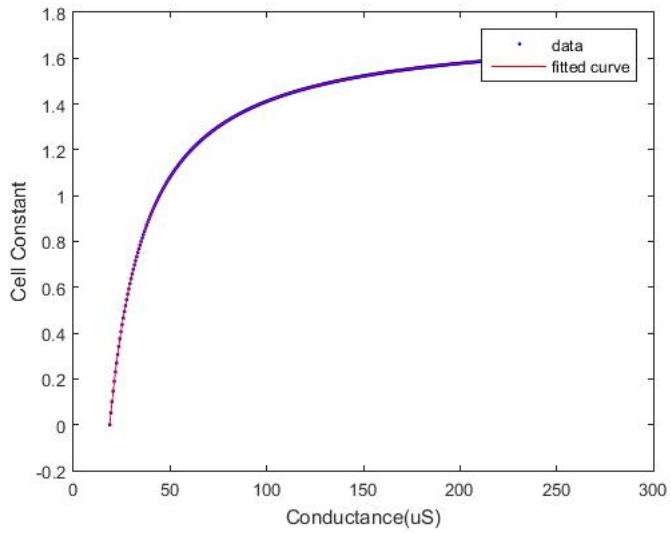

Figure 4.10: Cell constant as a function of conductance for conductivity values up to 400 μS/cm

The fit is really good in this case. The formula of the fitted curve is:

$$f(x) = \frac{p_1 x + p_2}{x + q_1}$$

The values of the curve factors are given in Table 4.4:

p_1	1.744
p_2	-32.75
q_1	0.376

Table 4.4: Curve fit factors

For a wider spectrum of conductivity values the results are shown in 4.11:

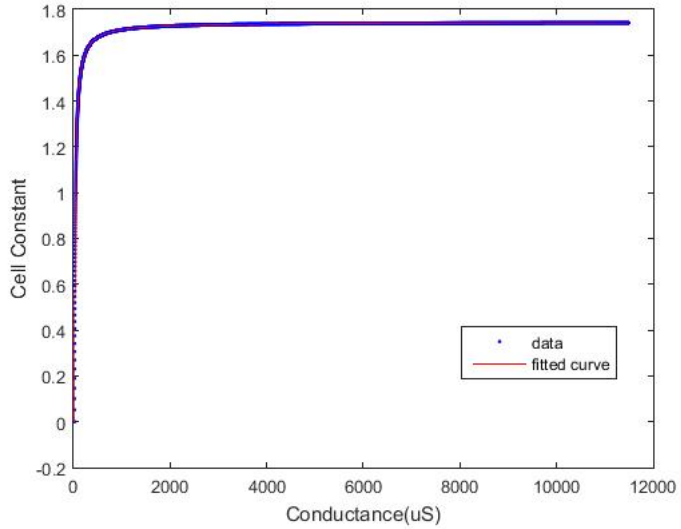

Figure 4.11: Cell constant as a function of conductance for conductivity values up to 20.000 μS/cm

The same curve as before is fitted to the data and the results are in Table 4.5

p_1	1.744
p_2	-32.75
q_1	0.376

Table 4.5: Curve fit factors

The results for both simulations are identical. So the cell constant is given by the previously mentioned formula.

In order to make sure that the results of the simulation have some credibility, there are some standards that the simulation must meet. The main index of the quality of the simulation is the quality of the mesh. A high mesh quality indicates that the simulation model is thorough enough to produce accurate solutions.

The mesh that was used was user defined and it consisted of two parts:

The first part is a free tetrahedral mesh on the electrodes. The element size of this mesh is equal to the thickness of the electrodes 35 μm.

The second part is also a free tetrahedral mesh covering the PCB plane and the water sample. The element size of this mesh is set to the predefined value of *Finer*.

Figure 4.12 shows the meshing of the simulation and Figure 4.13 shows the quality factor of the meshing. As it can be seen the minimum value is above 0.4 and this makes the meshing accurate enough for this simulation.

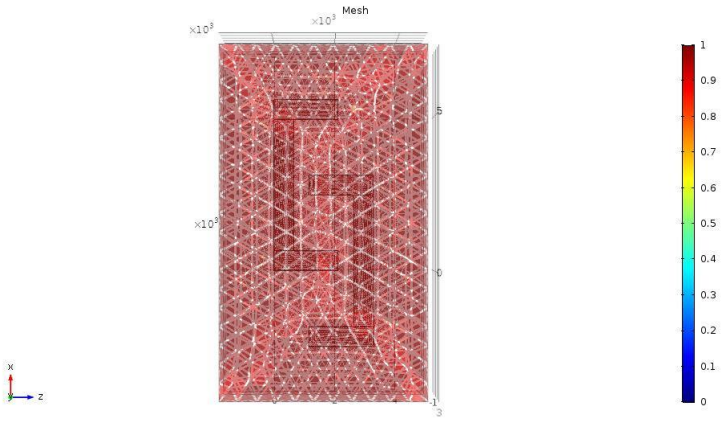

Figure 4.12: Depiction of the messing of the probe

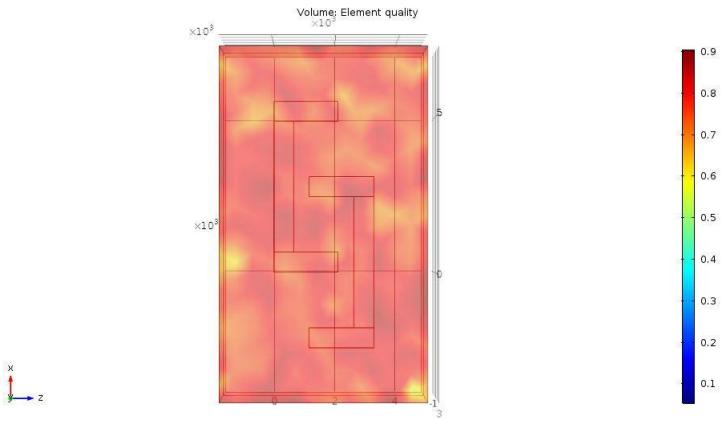

Figure 4.13: Quality of the meshing of the probe

4.2.8. Study of probe's characteristic dimensions

[28] suggests, the value of the cell constant depends on e physical quantities:

The length of the finger (**length**)

The space between the fingers (**s1**)

The width of the probe electrodes (**w**)

But by only considering those factors, one is left out. It is the **s2** attribute as seen in Figure 4.14.

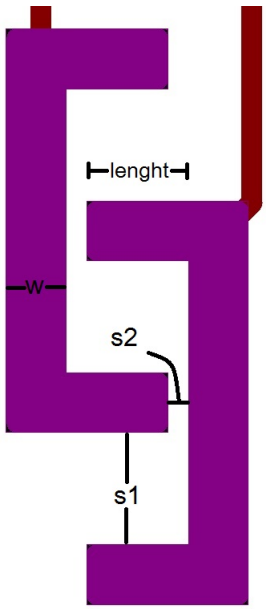

Figure 4.14: Characteristic dimensions of the probe

In order to understand better the dependency of the cell constant to the physical dimensions of the probe, a Matlab script (A.4)was used to iterate through all possible combinations of values for the four dimensions. For each dimension a spectrum of values was chosen. Table 4.6 shows the areas of the values:

Dimension	Range (μm)	Step (μm)
length	500 to 1100	150
width	200 to 950	150
s1	1000 to 2800	200
s2	200 to 800	150

Table 4.6: Curve fit factors

For each configuration, the simulation was run for a conductivity value of 400μS/cm, which is a value, common for tap water.

It would be ideal to provide a visualization of how exactly the cell constant for higher conductivity values depends on those characteristic dimensions. But since there are 4 of them, such curve cannot be plotted. What can be done instead is to present the cell constant dependence on each individual dimension keeping the other one fixed.

The next 4 figures show how each dimension impacts the cell constant of the probe. After fitting many different curves on the data there was on curve that fitted data on the 3 first graphs in the best way. It is the one used previously:

$$f(x) = \frac{p_1 x + p_2}{x + q_1}$$

Under each plot there is a table containing the values coming from the fit.

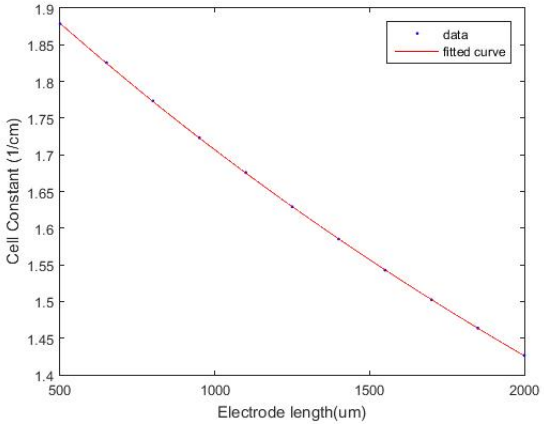

Figure 4.15: Cell constant plotted against the length of the finger

p_1	-0.5631
p_2	1.265e+4
q_1	6079

Table 4.7: Curve fit factors for variable finger length

As the length of the fingers increases, the cell-constant reduces. In the case of the parallel plates the cell constant is proportional to the distance, between the plates and inversely proportional to their distance. So in the present case, when the length of the fingers increases, so does the surface and so the cell constant decreases, almost in a linear way.

The same principle explains the behaviour of the other 2 diagrams.

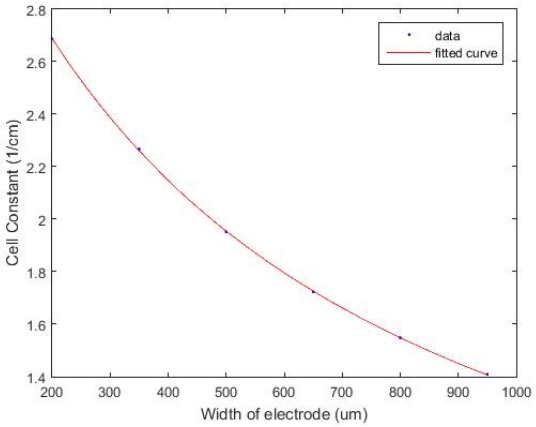

Figure 4.16: Cell constant plotted against the width of the probe terminals

p_1	-9.058
p_2	1.338e+5
q_1	6.655e+4

Table 4.8: Curve fit factors for variable width

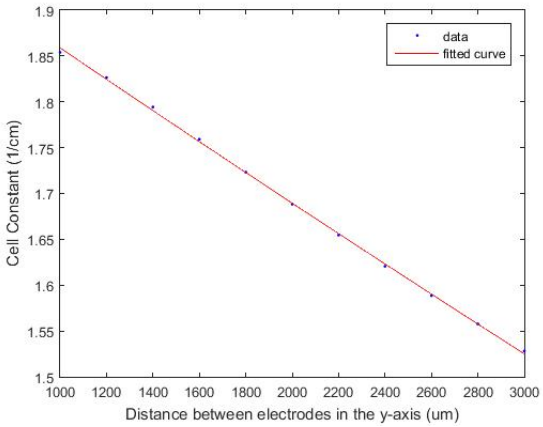

Figure 4.17: Cell constant plotted against the distance of the fingers on the y-axis

p_1	-9.216
p_2	1.289e+5
q_1	6.338e+4

Table 4.9: Curve fit factors

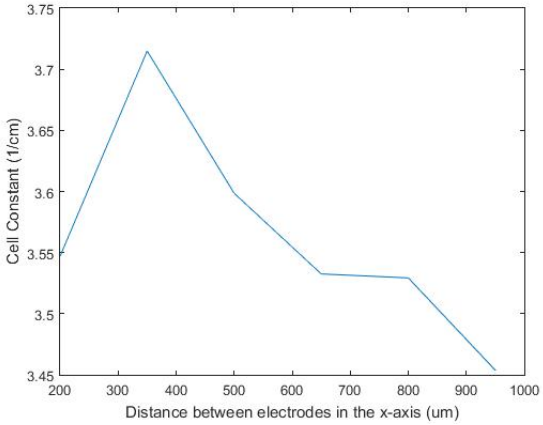

Figure 4.18: Cell constant plotted against the minimum distance between the two terminals on the x-axis

The last figure, shows an irregular contribution to the cell constant from the s2 variable. Further investigation in the acquired data, revealed that the behaviour of this specific variable is inconsistent and if the rest of the variables change, so does the equivalent plot of s2. It is important to note that [28] does not mention anything about this dimension.

4.3. Initial testing setup

In order to avoid the double effect from becoming dominant, causing damage to the device and uncertainty to the measurement, the voltage applied to the probe needs to be altering. In order to determine the frequency at which the phenomenon disappears

There were 3 different variations of the same probe made:

1. Unshielded
2. Shielded, with a back copper field connected to one of the signal terminals
3. Shielded, with a floating back copper field.

The probes were connected to the **Agilent 4294A Precision Impedance Analyser** with a coaxial cable in order to minimize the noise in the measurement. For this connection the probes were equiped with the SMA connector of Figure 4.19.

Figure 4.19: SMA connector

At this point it is interesting to notice the difference between what is simulated for the probe and what is expected from [28].

[28] comes up with an analytical formula to calculate the cell constant:

$$cell\ constant = \frac{\epsilon_0 \epsilon_r}{C}$$

$$C = (N-1)LC_1$$

$$C_1 = \frac{\epsilon_0 \epsilon_r}{2} \frac{K\left[(1-k^2)^{1/2}\right]}{K(k)}$$

$$K(k) = \int_{t=0}^{1} \frac{dt}{\left[(1-t^2)(1-k^2t^2)\right]^{1/2}}$$

$$k = \begin{cases} \frac{s}{s+w} & \text{for N=2} \\ cos\left(\frac{\pi}{2}\frac{w}{s+w}\right) & \text{for N>2} \end{cases}$$

where:

ϵ_0 is the permittivity of vacuum,

ϵ_r is the relative permittivity of the medium,

K(k) is the complete elliptic integral of the first order

s is the space between the electrodes as defined in [28],

w is the width of the electrodes as defined in [28],

L is the length of the "finger" as defined in [28],

N is the number of electrode fingers

A Matlab script A.2 was used in order to calculate the cell constant based on the previous equations.

The result of those calculations is 0.01. As it can be seen the difference is great, both in quantity and quality.

What [28] suggests is a fixed value, that implies an ohmic relationship between the voltage and the current, which is not true according to the findings of the simulations. The difference in quantity is also very big, if the cell constant for high conductivity values is taken into account.

4.4. Measurement Results

The experiment was conducted in room temperature (23oC). In order to test the probe, samples with different conductivity were necessary. In order to create such samples NaCl was dissolved in de-mineralized water. The solutions had the following NaCl concentrations: 0%, 0.035%, 0.07%, 0.105%, 0.14%, 0.175%, 0.21%, 0.245%, 0.28%, 0.315% and 0.35%. Afterwards the samples were measured with an accurate conductivity sensor. Table 4.10 shows how salinity values correspond to conductivity values:

Salinity (%)	Conductivity (μS/cm)
0	65
0.035	727
0.07	1425
0.105	2160
0.14	2760
0.175	3420
0.21	3990
0.245	4620
0.28	5190
0.315	5870
0.35	6220

Table 4.10: Dimensions of square parallel copper planes

The measured quantity was the conductance of each sample. For those measurements the option C_P-G of the **Agilent 4294A Precision Impedance Analyser** was used. There were three measurements made in order to calibrate the analyser:

open,

short-circuited and

using a known load, in this case 50 Ω.

The bandwidth of measurement was 350 Hz up to 1 MHz and the resolution used was 201 frequency points. The amplitude of the applied signal was 500mVolts.

The results obtained are given in Figures 4.20, 4.21, 4.22:

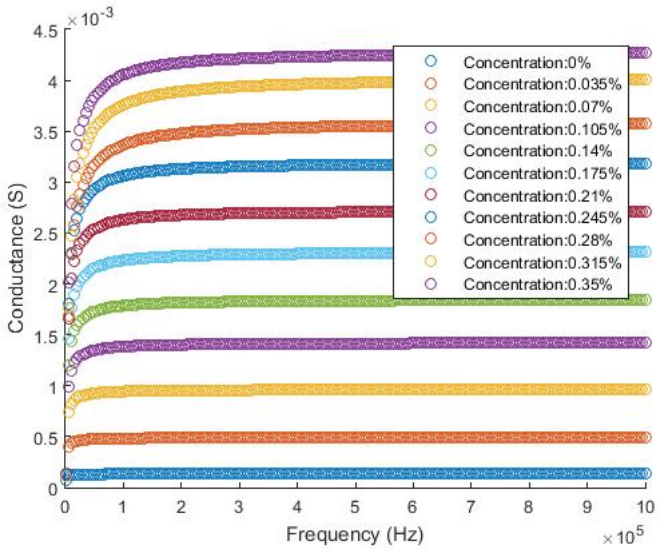

Figure 4.20: Probe design without shield

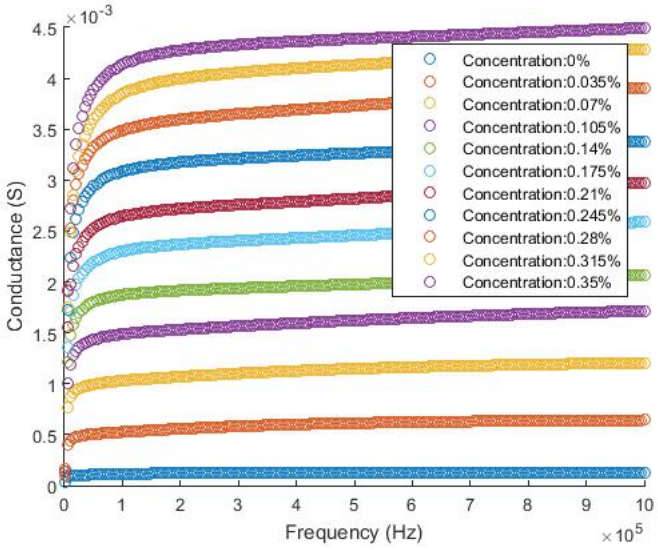

Figure 4.21: Probe design, back copper plane connected to one of the signal terminals

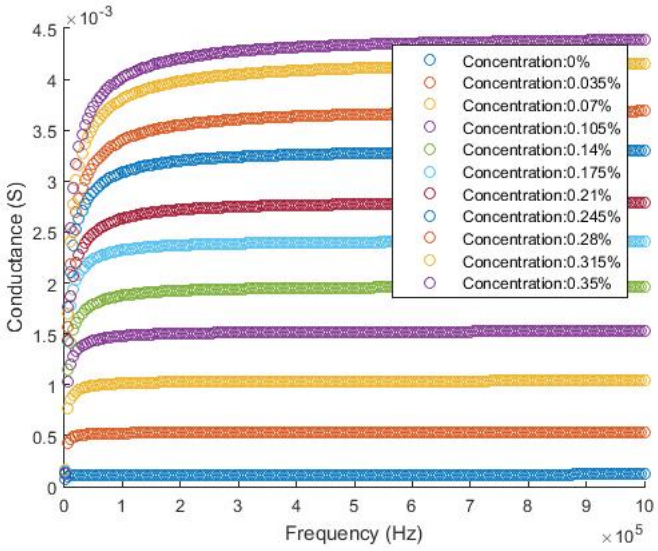

Figure 4.22: Probe design, back copper plane unconnected

There are mainly two pieces of information from the figures above:

1. The grounded shield has the worst performance, so the unshielded variant is chosen, since the results are similar and this way the design is simpler,

2. The frequency of the signal applied to the probe needs to be more than at least 250kHz in order to avoid the occurrence of the double layer effect.

In order to verify that the probe worked as expected a very simple measurement set-up, composed by a signal generator, set at 500mVolt amplitude and 350kHz frequency, an 1kΩ resistor, a multimeter and the samples described above.

Figure 4.23 shows the results obtained and compared with the results given by the **Greisinger GMH3431**:

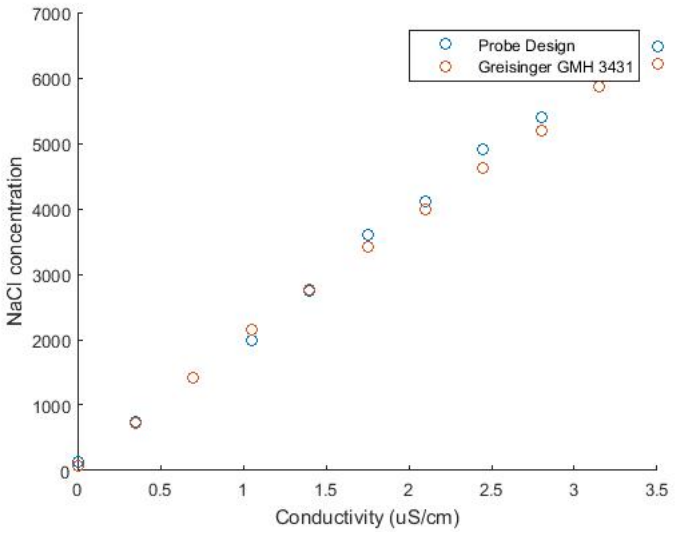

Figure 4.23: Probe design compared to Greisinger GMH 3431

The figure above allows to assume that the results of the simulations are useful and can be used in the way described above to measure conductivity.

Looking at Figure 4.23 it is noticeable that when the conductivity is increased so does the difference of measurement of the two probes. This can be easily explained. In all those calculations temperature is never taken into account for the probe design. On the other hand **Greisinger** compensates its measurement for temperature differences.

4.5. Conclusions

In this chapter various different probe topologies were simulated and their behaviour was simulated. After the analysis followed the reasoning behind the selection of the specific design and a more thorough study of the selected topology. The formula for calculating the "cell-constant" was given and the quality of the simulation was reviewed. Then the contribution of the physical dimensions of the probe to the cell-constant" was studied.

After the study of the probe an initial testing phase took place to solve questions regarding the stability of the measurement over different frequencies. There it was determined that the best possible probe configuration is the one that has no copper fill behind the probe.

Finally the probe was initially tested against another,l commercially available, accurate conductivity sensor and, without the temperature correction mechanism applied to the measurements of the probe the two data sets correlated rather well.

Those results allowed to show confidence to the simulation results and to use them in order to build the system.

5

Peak Detector

In order to determine the conductivity of water, an altering voltage signal is applied to the water. Then the signal going out of the water is measured and the drop of the voltage is then used to determine the resistance of the water. Figure 5.1 offers a visualization of the measurement:

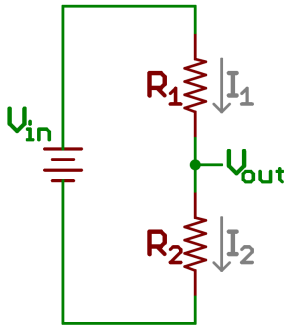

Figure 5.1: Voltage divider

In the above Figure R_1, V_{in} are known. By measuring the V_{out} R_2 is given by the following relationship:

$$R_2 = \frac{R_1}{\frac{V_{in}}{V_{out}} - 1}$$

Then, by inverting R_2 the conductance is found. Finally, using the results of the simulations, the cell constant, for that conductance can be calculated and the get the conductivity.

So the R_1, frequency and V_{in} values of the applied signal must all be determined during the design of the sensor.

The most important issue though is that of measuring the amplitude of the signal. This was one of the biggest challenges of the project. Due to the fact that the signal is altering and the frequency has to be higher of a certain value measuring the amplitude of this signal is not a trivial task. The conductivity measurement specification is set at the end of Chapter 1. So those are the requirements needed to be met.

In the following sections all the design choices made will be explained, offering an insight on the functions of the sensor.

5.1. Resistor's value

A crucial element that determines the sensitivity and range of the sensor is the value of R_1. This is because the output voltage is given by the following formula:

$$V_{out} = \frac{R_2}{R_1 + R_2} V_{in}$$

As it can be seen if the value of $R_1 \gg R_2$, then the output voltage would be almost zero.

On the other hand if $R_1 \ll R_2$ then there is no voltage drop observed and the measurement is again useless.

So the selection of a proper resistor is of great importance. Another important fact to be taken into account at this point is that the voltage measurement's accuracy decreases when the the difference of the two values increases. In this specific case, it means that there is a limit on the water resistance that can be measured, depending on the value of R_1.

Since the sensor is purposed for measuring conductivity values that appear in irrigation and urban water consumption, it was decided that the measurements should be very accurate on the lower band of conductivity.

The measurement set, described in Chapter 4, provided the following results:

Salinity (%)	Conductivity (μS/cm)	Resistance (Ω)
0	65	10600.0
0.035	727	2222.2
0.07	1425	1148.1
0.105	2160	812.5
0.14	2760	589.0
0.175	3420	450.0
0.21	3990	394.2
0.245	4620	330.3
0.28	5190	300.4
0.315	5870	260.9
0.35	6220	250.0

Table 5.1: Resistance of various NaCl concentration solutions

Based on those results and due to the need to be accurate at low conductivity values and at the same time have a sufficiently large spectrum of measurement it was decided that R_1 will be 1kΩ.

In order to increase the accuracy and the spectrum of measured values, more resistors could be used in parallel and, using switches change between them automatically, according to the sample under examination.

5.2. Frequency

In order to avoid the appearance and the interference of the double layer effect, the frequency needs to be above a certain value. Using the results of the measurements from the previous chapter and especially the findings of Figure 4.20, it was determined that the frequency needs to be at least above 200kHz and as high as possible.

Initially the decided frequency was set to 500kHz. This is a rather profound choice, based on the results shown on the previously mentioned figure.

Nevertheless, the frequency that is currently applied on the sensor is 300kHz. This decission was made because of the fact that the original waveform generator generates square waves and a filter is used to transform the signal from square to sinusoidal. So in order to create a sinusoidal signal with the least possible distortion, the frequency needed to be reduced.

5.3. Passive Peak detector

This section presents the different methods that were examined in order to decide on the most suitable peak detector for the sensor.

5.3.1. Peak detection using a diode

One of the most common way to perform peak detection is using a diode and a capacitor.

Figure 5.2 shows how exactly the peak detection is done:

When the signal is in the positive part of the period the diode conducts and the capacitor is charged.

When the signal is in the negative part of the period the diode does not conduct and the capacitor is discharged.

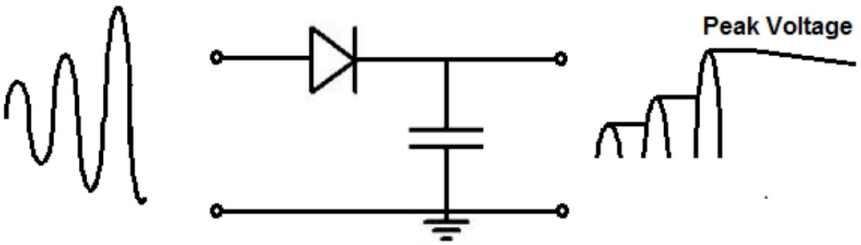

Figure 5.2: Diode Peak detector

In order to rectify the signal in the best possible way, the capacitor needs to be of sufficiently high capacitance, in order to discharge slowly for a given load, until it gets charged again on the next period.

For low frequencies this very simple circuit can rectify a signal. In case of high frequencies though several problems occur. If the value of the capacitor is too big then it will never fully charge, if the value is too low, then the capacitor is discharged very fast and the output is not stable.

Another important fact is that the output voltage is reduced by a portion equal to the forward voltage of the diode.

5.3.2. Active Peak Detector

A circuit that cures the last problem from before is shown in Figure 5.3.

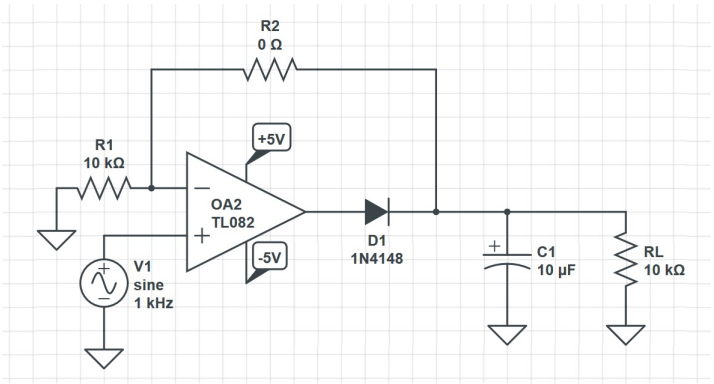

Figure 5.3: Feedback Loop Peak Detector

The performance of the above circuit is extremely improved compared to that of the passive peak detector. As it was said before the negative feedback loop cures the issue of the voltage drop on the diode providing a better and more linear peak detector.

But this peak detector limits the frequency that can be used. This is due to the slew rate of the OpAmp. The slew rate is measured in V/ms and it indicates how fast can an OpAmp switch voltage on the output depending on the input.

On this application, as it was said before the initial frequency requirement was set to 500kHz. LTSpice simulations were used in order to determine the performance of this peak detector.

Figure 5.4 shows the simulated circuit. In this case input is the signal that is under measurement and output is the value of the measurement obtained. Since the ratio V_{in}/V_{out} is important in calculating the resistance of the water, it is crucial to have an analogy between the signal under measurement and the final voltage measurement.

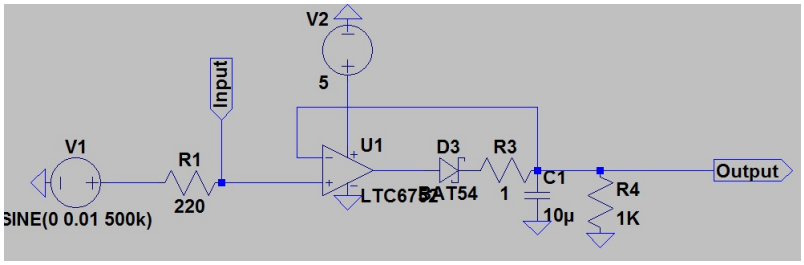

Figure 5.4: Feedback Loop Peak detector, LTSpice simulation

Figure 5.5 shows the relationship between the signal measured and the final measurement and it is not linear, especially in the lower range of input voltage (high conductivity values).

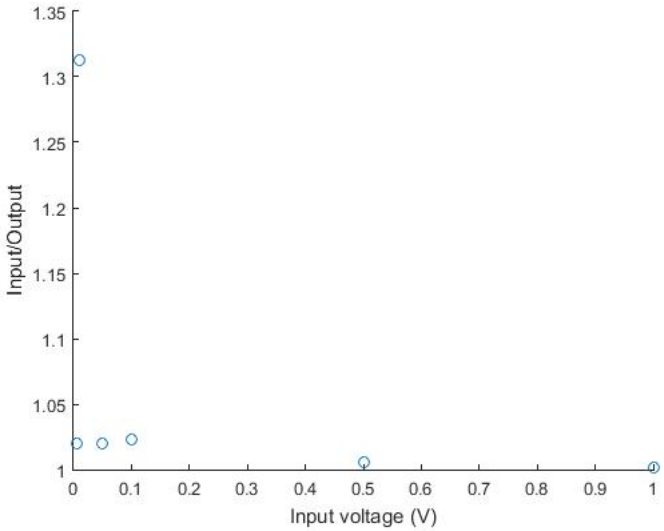

Figure 5.5: Feedback Loop Rectifier

5.3.3. Improved Peak detector

[40] suggests two circuits that can improve the result of the measurement. Both solutions were simulated and tested again with the help of LTSpice.

Figure 5.6 shows the first suggested circuit. In this circuit the rectifying diode is replaced with a Schottky diode. This way the voltage reduces the forward voltage drop, increasing the current that charges the capacitor. A matched Schottky diode is used in the feedback loop of U1 in order to compensate for the bias voltage drop of the rectifying Schottky diode. In the input a Schottky diode is used again to drive the negative voltage of teh signal to 0, in order to avoid the usage of negative power supply to the OpAmpS.

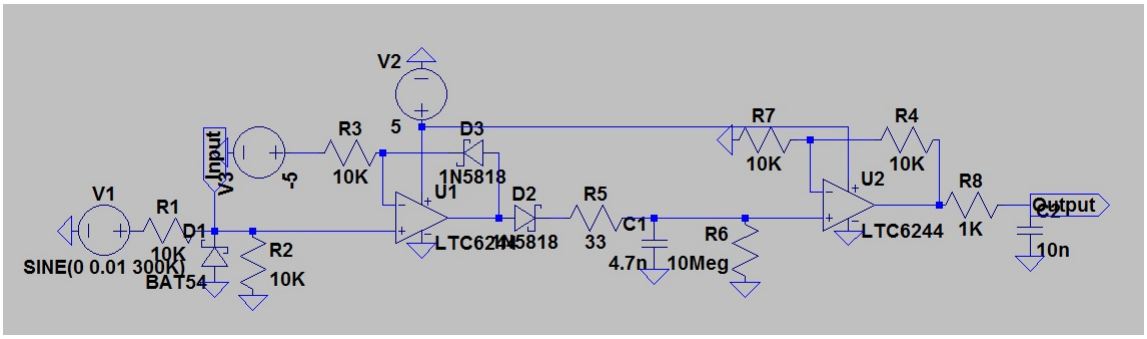

Figure 5.6: Improved peak detector

The results obtained from the simulation are shown in Figure 5.7.

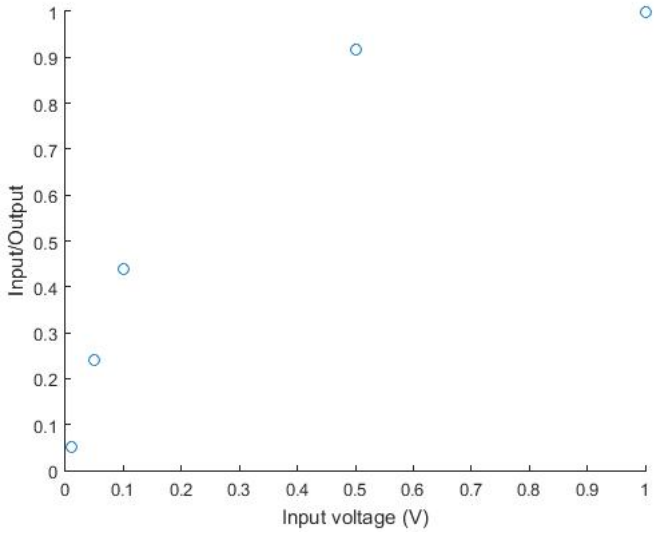

Figure 5.7: Improved peak detector simulation results

The advantage of this circuit is the lower voltage drop, due to the Schottky diode and hence the less time it takes to charge the capacitor.

5.3.4. Current Boosted Improved Peak Detector

The second solution that is supposed to improve the peak detection given in [40] is shown in Figure 5.8. In this case the Schottky diodes are replaced by matched NPN BJTs, that can charge the capacitor even faster than the previous circuit.

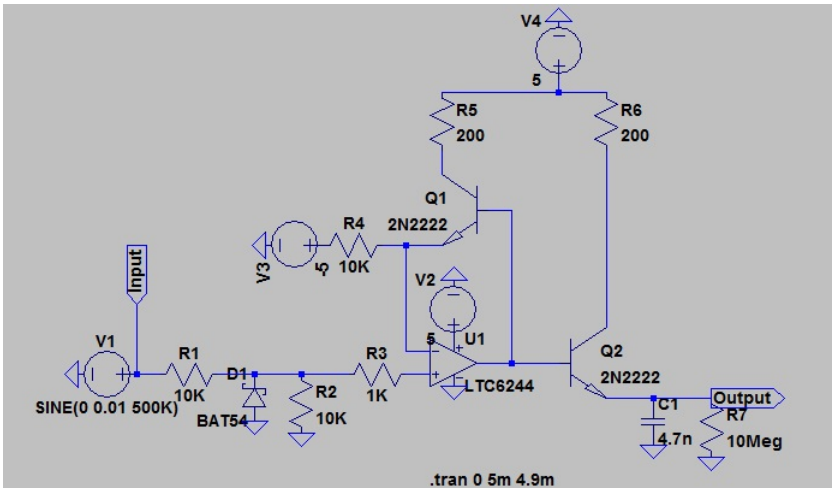

Figure 5.8: Current Boosted peak detector

The results of this simulation are shown in Figure 5.9. As it can be seen there are is almost no difference from the solution, for the given working frequency.

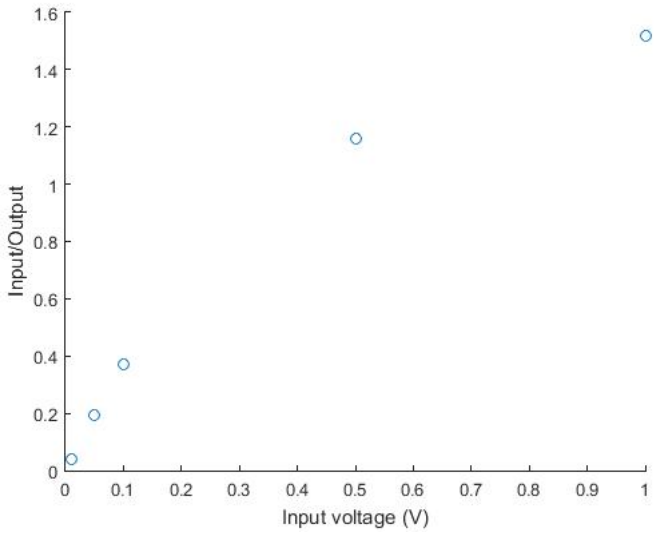

Figure 5.9: Current Boosted peak detector simulation results

Both of the suggested methods brought up very poor results. When the conductivity was getting lower there was minimum value that they could read and then the result of the measurement was no longer relevant to the input.

5.3.5. LTC1968 RMS to DC Converter

The option that was reviewed and finally approved was the chip described in [38]. The function of this chip fits exactly the needs of this project. This chip accepts an altering voltage signal as input and outputs the RMS value of the input.

In order to convert the altering signal to a DC value this chip uses a multiplication/division block. The input signal is multiplied/divided with the output signal and then driven through a low pass filter in order to obtain only the DC component of the multiplication result.

At this point it is important to note that when the signal is applied to water, only the amplitude of the signal is affected and not the frequency and so the multiplication will contain a DC component and harmonics of the frequency of the original signal.

The function of this chip was simulated using LTSpice as well.

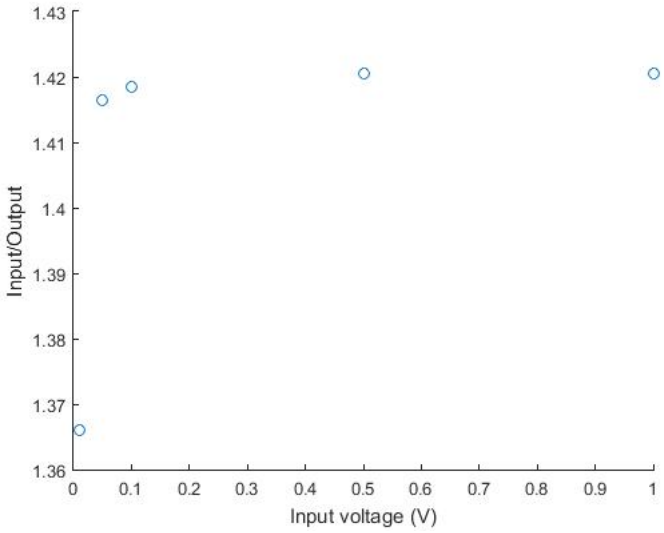

Figure 5.10: LTC1968 simulation results

As it can be seen this solution also suffers in the side of voltage values. Simulations suggest that there is a stabilization time for the measurement to be correct. This time is 3 μs.

5.4. Conclusions on the Peak Detector

Based on the results of the simulations there are only two candidates that seem to perform in an acceptable way, regarding to the needs of this project, namely the *Active peak detector* and the *LTC1968*.

In order to decide which one of the two peak detectors produces more consistent results, more input voltage numbers from the lower band of the spectrum were used.

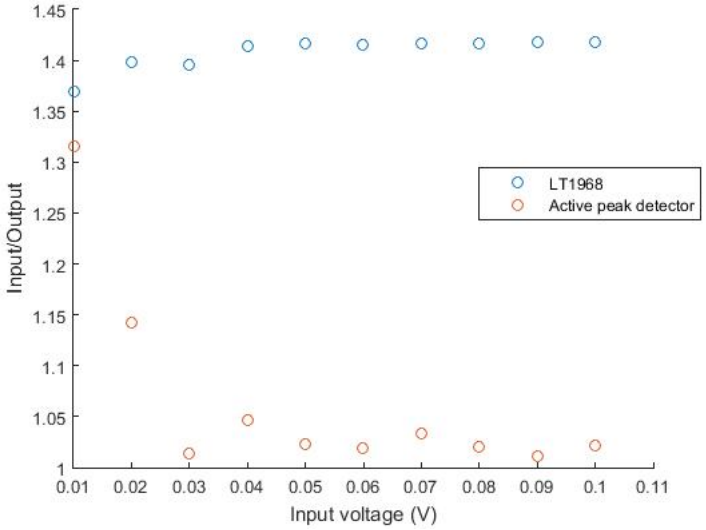

Figure 5.11: Comparison between LTC1968 and active diode rectifier

From Figure 5.11 it is easy to see that the LTC1968 is more stable compared to the active diode peak detector.

After the simulations, the two peak detectors were also tested in reality. There it was found that the active diode peak detector's performance was worse than the simulation and thus it concluded that the LTC1968 should be used.

It can be also seen that LTC1968 performs better (more stable) for lower voltages (higher conductivity values) compared to the active peak detector. This allows the LTC1968 to be more accurate in this side of the spectrum of values.

Another advantage of the LTC1968 is that the difference between the actual value of the peak and the measurement is of an almost fixed factor of $\sqrt{2}$, which makes calculations a lot easier, when working with fractions.

6

Temperature Compensation

6.1. Temperature sensor choice

Conductivity is strongly dependent on the temperature. For this reason all the measurements in bibliography are made converted to a reference temperature, which usually is 25°C. So in order to measure the conductivity it is important to also measure the temperature of the sample. [8] suggests the following temperature compensation formula:

$$c_{25} = \frac{c_\theta}{1 + (a_{\theta,25}/100)(\theta - 25)}$$

where

c_{25} is the conductivity calculated for 25°C.

c_θ is the measured conductivity.

$a_{\theta,25}$ is the temperature coefficient, equal to 2 for water.

θ is the temperature of the sample.

There are several different methods in order to measure the temperature of a sample. Some key factors in selecting the sensor in order to measure the temperature are:

The range of measurement.

The accuracy of the sensor.

The calibration procedure.

The cost.

It is important to note that due to the needs of the project the measurement has to be made on-chip and the sensor needs to be in physical contact with the sample due to the specifications of the conductivity sensor and in order to acquire maximal accuracy. For this reason only relevant techniques are reviewed. It is also important to note that IC temperature sensors are not considered as candidates for the project, because the sensor needs to be immersed inside the water. In order to do that the IC sensor would need to be insulated, meaning that the it would not be in direct contact with the sample. A way to use them in this case is by creating a metals surface that on one side resides the sensor and on the other it is in physical contact with water. This chapter review the different temperature sensors available and describes in detail the calibration process and results of the selected sensor.3

6.1.1. Thermistor

Thermistor's name is the combination of the words thermally-sensitive resistor. This resistor changes its resistance to the flow of electric current, when exposed to changes of temperature.

Figure 6.1: Common thermistor packaging

Thermistors are a type of semiconductor. There are two types of thermistors:

- The NTC (negative temperature coefficient) and the
- PTC (positive temperature coefficient).

The temperature coefficient shows how much does the resistance change with the temperature. An NTC (negative temperature coefficient) thermistor will have its electrical resistance decreasing with the increase of the temperature. A PTC (positive temperature coefficient) thermistor will have its resistance increased with the increase of the temperature. According to [29] NTC thermistors are usually used in order to measure the temperature.

A thermistor is usually made out of ceramic materials. A small piece of this material is usually contained in glass or epoxy in order to protect the sensor. Epoxy coating offers some protection against humidity and corrosion. The thermistor itself has a very small size in order to minimize the response time in temperature changes.

One downside of the thermistors is that the relationship between temperature and resistance describing them is in general not linear. But according to [13] when the thermistor is used in series with a resistor as part of a voltage divider the current obtained due to the voltage applied is linear to temperature.

Thermistors can measure temperatures between -50 ^{o}C and 300^{o}C with an accuracy of $\pm$0.1^{o}C.

Thermistors are cheap, easy to use, those in epoxy can be used for measurement directly in the water, but they need to be calibrated.

6.1.2. Resistive Temperature Detectors

[39] informs that RTDs are high precision temperature sensors, made from high purity conducting metals, with platinum being the most commonly used.

Generally there are two different RTD sensor configurations: the wire wound and the thin film.

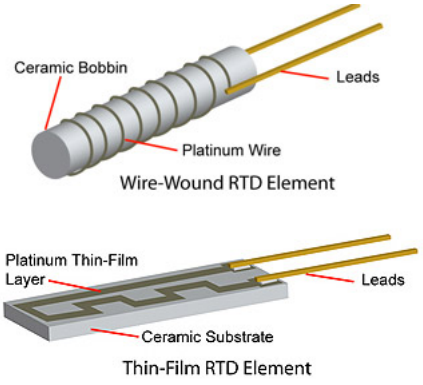

Figure 6.2: The two RTD configurations

Wire wound configuration uses either an inner coil or an outter coil as RTD. In the first case the coil goes through a ceramic plate from a hole, while in the second case the coil is wrapped around a ceramic or glass cylinder. In both cases the measured quantity is the resistance of the coil, which is associated with the temperature.

According to the previous source: *"Thin film sensors are made by a thin layer of resistive material deposited onto a ceramic substrate. A resistive meander is etched onto the sensor and laser trimming is used to achieve the nominal values of the sensor"*.

Thin film RTDs have several advantages over wire RTDs:

- They are cheaper.
- They have smaller dimensions.
- Due to their smaller dimensions they adjust faster to the ambient temperature.

Compared to the thermistor film RTDs can be more accurate, have a greater temperature range and be linear, but they are more expensive and they have a longer response time.

6.1.3. Thermocouples

A thermocouple, according to [19] is a sensor that uses the junction of two wires of different metals in order to measure the temperature. The wires are welded together at one end and the voltage difference measured between their other end is related to the temperature. This output is a small signal.

There are several different types of thermocouples available.

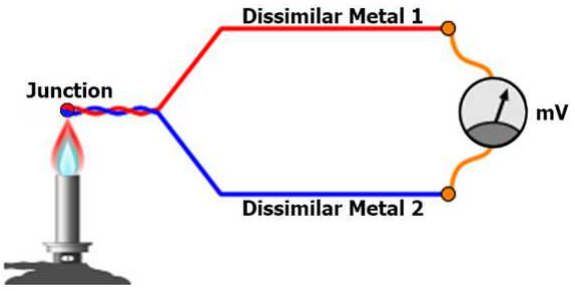

Figure 6.3: Typical thermocouple configuration

Different thermocouples have different qualities, such as temperature range and accuracy. The types of thermocouples are:

- J, K, T, E known as "Base Metal" thermocouples and
- R, S, B known as "Nobel Metal" thermocouples

Thermocouples can have a huge temperature range. For example type K, which is the most common thermocouple used, has a range between -270^{o}C and 1260^{o}C. Type B can measure from 0^{o}C up to 1700^{o}C, which is the highest temperature that those sensors can measure. Those ranges are nominal and whether a thermocouple can actually measure the whole range of measurement depends in the thickness of the wire.

There are 4 different sensor configurations:

1. Grounded Thermocouples: Here both the wires and the sheath of the sensor are welded together at the tip of the probe. This configuration guaranties short response time, since the sensor is in physical contact with the sheath, allowing heat exchange to happen more quickly. The wires are protected inside the sheath from corrosion, but it is more susceptible to noise due to the sheath.
2. Ungrounded (Common) Thermocouples: The wires are welded together, but there is insulation separating them from the sheath.
3. Exposed Thermocouples: In this configuration the junction is exposed to the environment. This makes the response time minimal, but it leaves the junction exposed to corrosion and degradation.

4. Ungrounded Uncommon: The wires are insulated from the sheath and from each other.

As said before thermocouples are the most commonly used sensors, due to the wide range of measurement, as well as due to the fact that they are extremely cheap. Compared to RTD sensors, they suffer in linearity and accuracy, but they achieve greater response time. In comparison to thermistors ([6]) a thermocouple is less accurate and less stable over time.

6.1.4. Comparison

Table 6.1 compares the parameters of the three different kinds of sensors:

	NTC thermistor	RTD	Thermocouple
Range	-50 up to 300^{o}C	-250 up to 900^{o}C	-270 up to 1700^{o}C
Accuracy	±0.1^{o}C	±0.01^{o}C	±0.5^{o}C
Linearity	Non-Linear output, Requires linerization	Linear	Non-Linear, Requires calibration
Stability	Good	Very Good	Bad

Table 6.1: Comparison table between temperature sensors

6.1.5. Final Choice

Conductivity measurement in water samples means that the examined sample will have temperatures varying from -2^{o}C up to 40^{o}C. So taking into account this, as well as all the advantages and disadvantages of the methods mentioned above, using a thermistor has the best trade-off between accuracy, linearity and cost at this range of temperatures.

Specifically the thermistor used at this point is the **NTCLE300E3502SB** Figure 6.4. This thermistor was chosen due to the fact that it is covered with epoxy, its price and its availability.

Figure 6.4: NTCLE300E3502SB thermistor

This temperature sensor is used as part of a voltage divider, in order to make the calibration easy. The value of the fixed resistance was picked to be 3kΩ. The value was chosen so that at 50^{o}C the voltage of the thermistor will be 2 Volt. This maximizes the dynamic range of the ADC of the chip. Figure 6.5 shows the temperature sensor's circuit. The 10nF capacitor is used to reduce the noise of the signal.

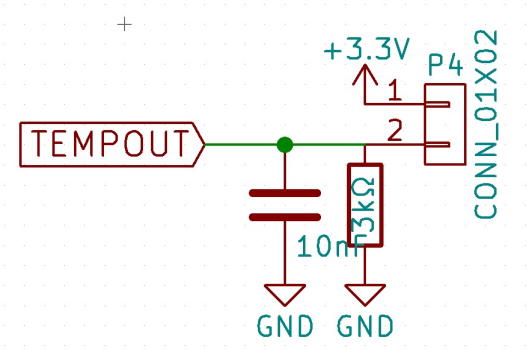

Figure 6.5: Sensor Circuit

6.2. Calibration Method

For the calibration of the sensor tap-water water mixed with NaCl was cooled down. Measurements were done from -2°C, when there was no ice pieces left in the sample, and heated-up until 45°C. Using the **Digitron 3204 Pt** temperature sensor, as well as the **VWR Hotplate/Stirrer** the sample was heated and stirred in order to make sure that the temperature is the same in all the volume of the sample. Both the sensor under calibration and the **Digitron 3204 Pt** were immersed equally deep inside the water sample, in order to achieve maximum accuracy. Figure 6.6 shows the calibration set-up.

The water sample was slowly heated and the voltage applied on the thermistor was measured every 0.5°. The results of the measurement are shown in Figure 6.7.

Figure 6.6: Calibration set-up

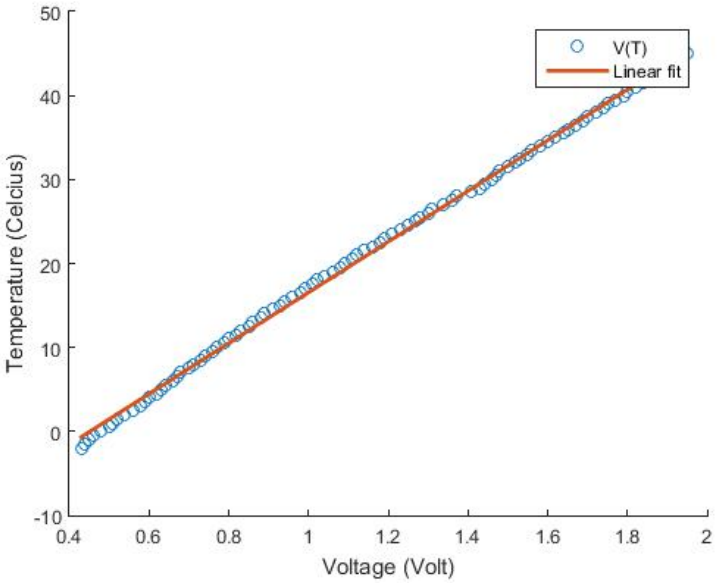

Figure 6.7: Calibration curve

Fitting a line y=αx+β on the measurement points gave the following results:

α	30.2±0.1 ^{o}C/Volt
β	13.7±0.1^{o}C
R^2	0.999

Table 6.2: Comparison table between temperature sensors

As it can be observed from the value of R^2, there is very high correlation between the measurement points and the linear fit of the data. So the following relationship can be used in order to convert voltage (Volt) into temperature (^{o}C).

7

Implementation of the system

The system consists of two basic components:

- The sensor
- The Android Application used for the read out

7.1. The sensor

The sensor itself can be viewed as a total of several modules:

- Micro USB connector
- 3.3V voltage regulator
- 5V voltage boost converter
- Voltage inverter
- The micro-controller
- The battery charging module
- Analog signal generator and read-out signal
- The temperature measurement circuit
- IC temperature sensor (not used in the current setup, but placed for future use)
- RGB led and pull up resistors for the I2C bus
- Accelerometer (used as an activation mechanism, not used currently)

7.1.1. Micro-USB connector

One of the most common connectors is the micro-USB connector, found in most portable devices nowadays. The currently used connector is also waterproof, due to the particular needs and usage of the sensor. Figure 7.1 shows the pin-out of the connector.

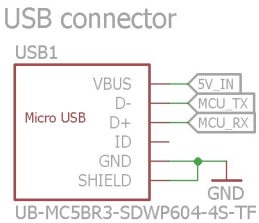

Figure 7.1: Voltage regulator block diagram

The Tx/Rx pins are not currently used. For serial communication an external module is used at the moment.

7.1.2. 3.3 Voltage regulator

The input voltage from the USB is 5V, but the micro-controller needs 3.3V as input. For that reason a XC6220B331MR-G is used as voltage regulator. Figure 7.2 shows the block diagram of this module:

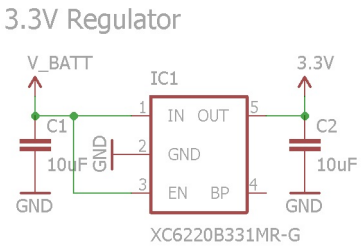

Figure 7.2: Voltage regulator block diagram

This regulator offers a very low drop out voltage, it operates in a temperature spectrum between -40C^{o} and 85C^{o}.

7.1.3. 5V Voltage boost converter and 5V inverter

The RMS converter, that is used to convert the AC output of the read-out signal to DC, operates under 5V. Also OpAmps operate between +5V and -5V volts, in order to be able to create and buffer both parts of the sinusoidal signal accurately, although it is not necessary, since the signal is limited to 3.3Volts.

In the case of the RMS converter, the input voltage needs to be as stable as possible. In order to achieve that, a boost converter and an inverter are used. The boost converter is the LTC3525.

The applied signal has also a negative voltage and for that reason, the OpAmps, that are part of the measurement and readout circuit, need to have a negative voltage as well, in order not to cut-off the part of the period that the voltage is negative. For that reason the The voltage inverter is the LM2664 Voltage converter is used in order to invert the 5Volts.

The circuits of the 2 components are shown in Figures 7.3 and 7.4:

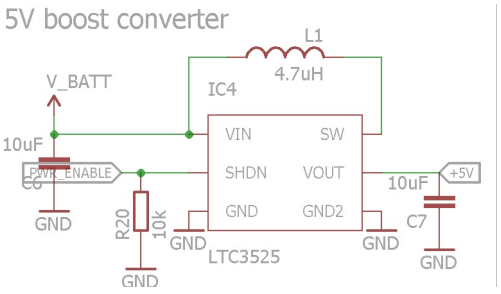

Figure 7.3: 5V boost converter

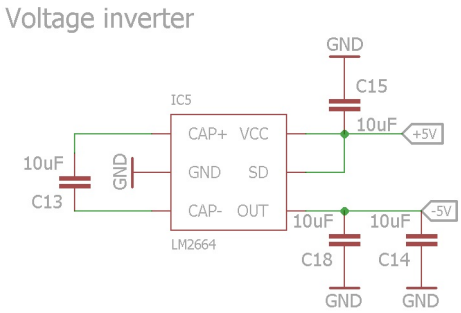

Figure 7.4: -5V inverter

7.1.4. The micro-controller

The micro-controller of choice is the Nordic **NRF51822**. This micro-controller can provide all the processing power necessary for the needs of the sensor and further more it has native BLE capabilities. This last feature was the concluding factor for the selection of the sensor, since BLE usage is an important requirement for this project. The

In order for the NRF module to be able to transmit and receive BLE packets, it is necessary to use the appropriate antenna. The need for really compact size sensor was the main cause of selecting the 2450AT18A100 Mini 2.45 GHz Antenna. For the antenna to work it is necessary to use balun filter. A commonly used such filter for Nordic chips is the 2450BM14A0002 2.45 GHz Impedance Matched Balun-Filter.

An RGB LED is also used for optical feedback and deluging (Figure 7.5):

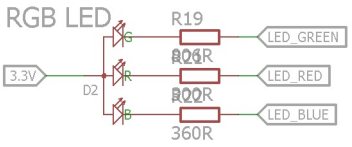

Figure 7.5: NRF51822 block diagram

Figure 7.6 shows the micro-controller, the BLE antenna, as well as the various other electrical components necessary for them to work, such as crystals, capacitors etc.

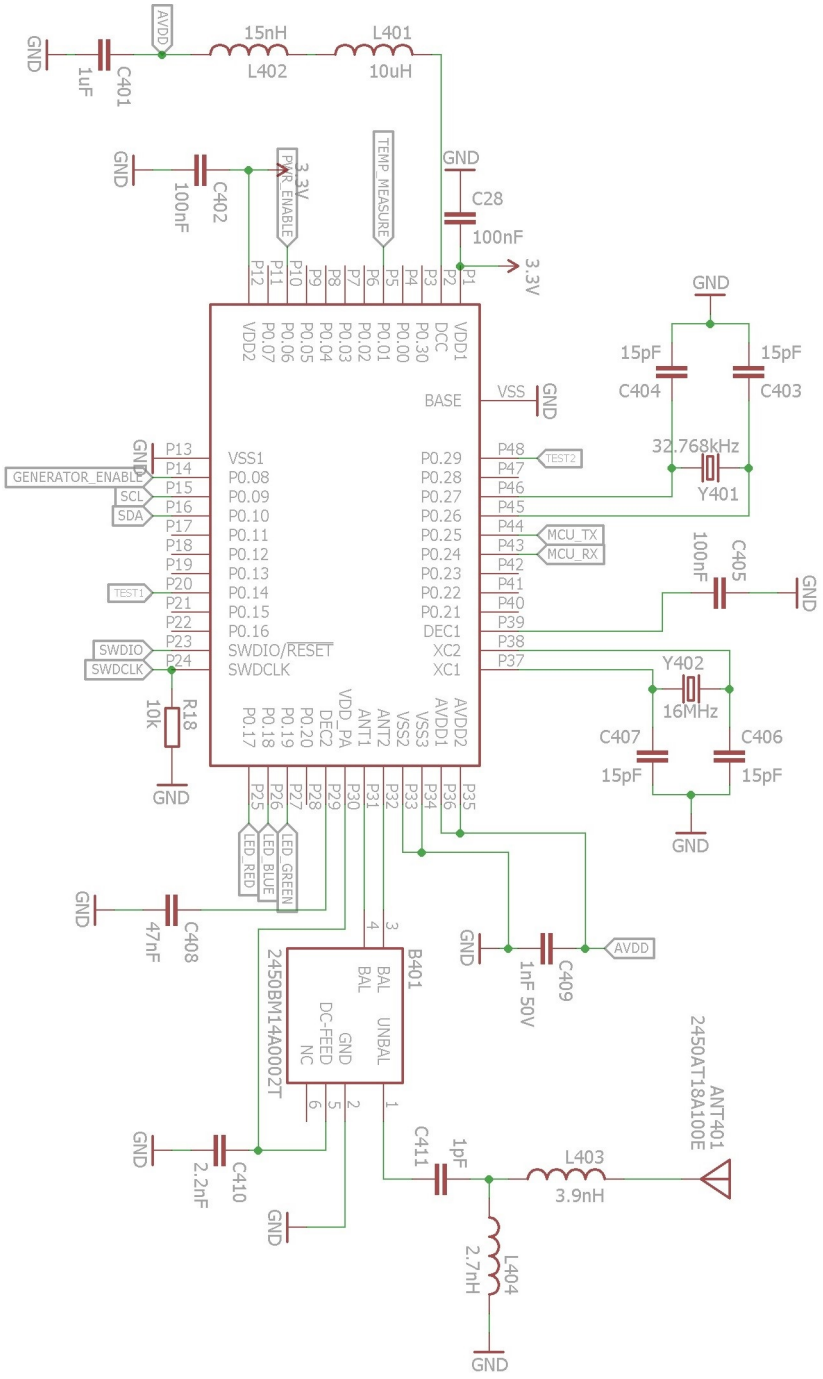

Figure 7.6: NRF51822 block diagram

7.1.5. The battery charging circuit

In order to charge the battery a charger circuit is necessary. For the needs of this sensor a 3.7V, 800mAh battery is used. The charge management controller used is MCP73831. This component is small in size and can operate between -40°C and +85°C.

Figure 7.7 shows the charge management controller and its surrounding circuit:

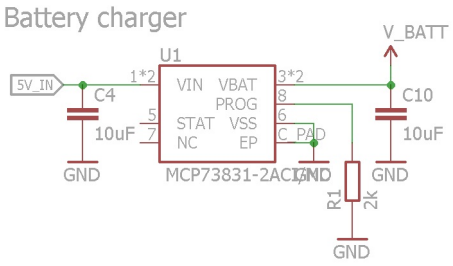

Figure 7.7: MCP73831 block diagram

7.1.6. Analog circuit

The analog part of the circuit can be seen as two different components:

The signal generator fed to the probe

The read-out from the probe

Analog signal generator circuit

In order to create the signal that is fed to the probe a square-wave signal generator is used. The signal is then passed by an appropriate filter that gives out a sinusoidal signal. LT1722 OpAmp is used in that filter, due to its high slew rate, in order to have a sinusoidal signal of minimum distortion. Using LTSpice to simulate the circuit, the results can be seen in Figure 7.8:

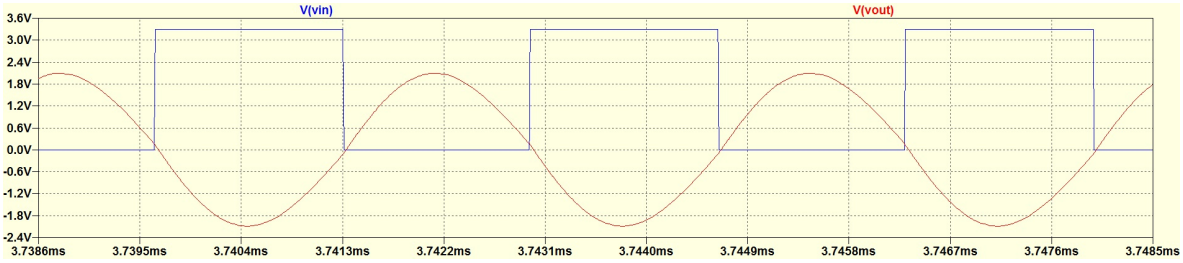

Figure 7.8: Transform square wave to sinusoidal

LTC6244 OpAmp is used in order to buffer the signal to the probe. This step is not necessary, but it provides a greater stability and accuracy to the signal on the probe.

It is important to clear out that the voltage applied to the probe, is also measured[1], since it is important to have an accurate measurement of that value as well, in order to calculate the conductance with the highest confidence. So the signal can either be fed to the probe or to the read-out circuit directly using a switch controlled by the micro-controller, in order to perform that measurement.

Read-out Circuit

In order to measure voltage of the probe, the peak detector that was described before is employed. The second OpAmp of the LTC6244 is used again, in order to buffer the signal to the LTC1968 RMS-to-DC converter. Then the DC voltage is fed to the MCP3421 ADC. Although the analog to digital conversion could be done by the micro-controller, this component is used, in order to achieve the maximum possible accuracy and also because it can be placed near the LTC1968, reducing the length between the output and the converter, hence achieving the best possible outcome. Finally the measured value is sent to the micro-controller, via I2C.

The analog circuit can be seen as a whole in Figure 7.9:

[1]The currently tested system did not employ this part, because it was deemed unnecessary at this stage.

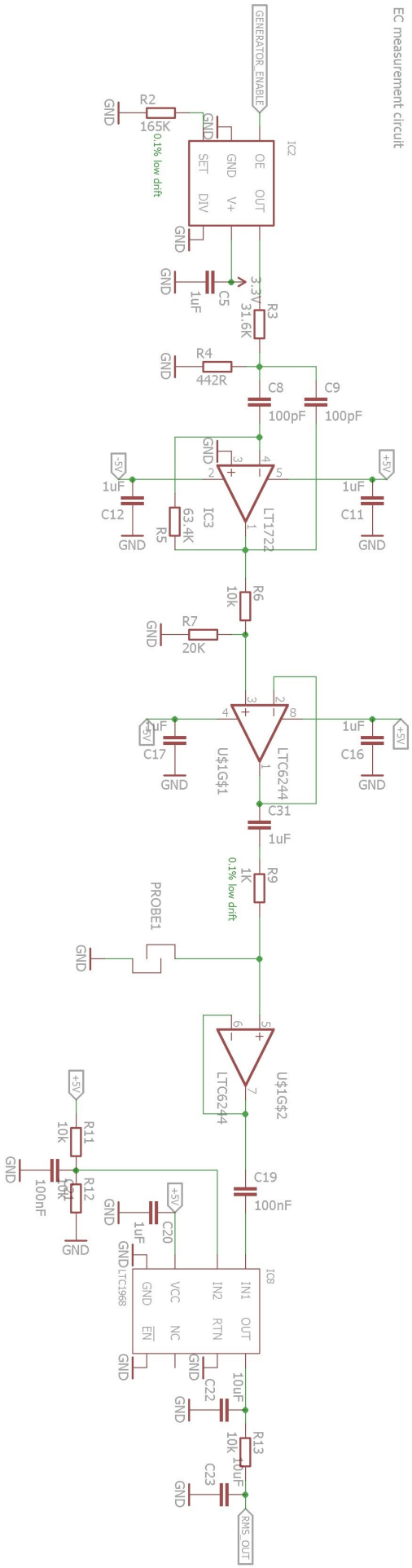

Figure 7.9: Analog circuit

7.1.7. Temperature measurement circuit

The last component of the sensor is the thermometer. The method to measure temperature is described thoroughly in Chapter 6. The block diagram of this module is shown in Figure 7.10:

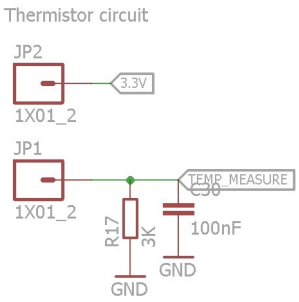

Figure 7.10: Temperature read-out circuit block diagram

Figure 7.11 shows the first working prototype built.

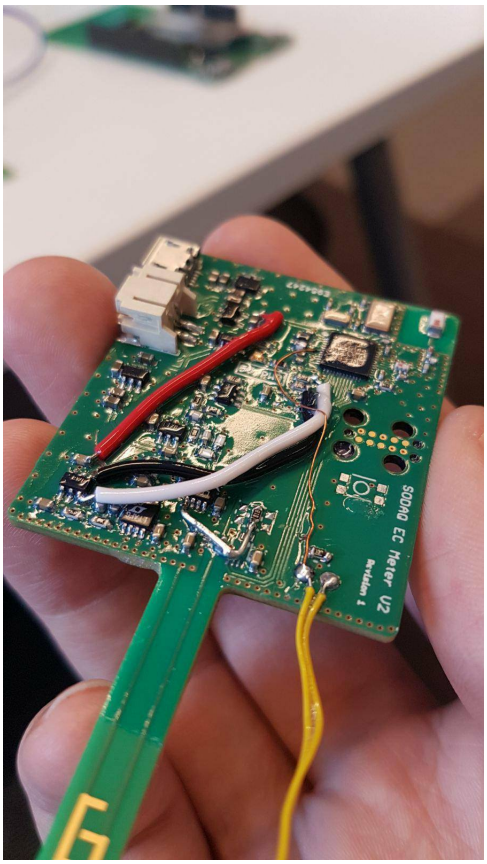

Figure 7.11: Fully functional sensor prototype

7.2. Android Application

In order to make the sensor compatible with current technology, an Android application was developed, in order to communicate and control the sensor, providing flexibility to the usage of the device. The Android app itself can be divided in three different modules:

The main user interface

The sensor id registration

The calibration interface

The interface that provides the user with more data regarding

The main aim of the application is to provide the user, with a clean, simple and easy to use interface, that will allow him to use the sensor in the easiest way possible.

7.2.1. Main User Interface

The main user interface consists of a button that when pressed, will send a message, addressing a specific sensor and will print the result of the measurement of the conductivity and the temperature. Figure 7.12 shows the main user interface:

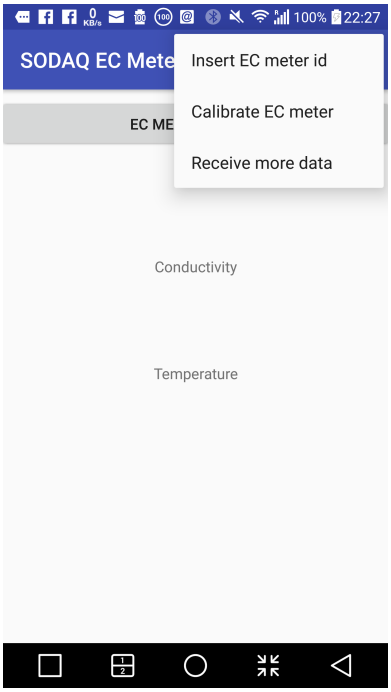

Figure 7.12: Android app: Main User Interface

Furthermore from this interface the user can access a menu that can take him/her to the other modules of the application.

7.2.2. Register Sensor

In order to avoid the incident of addressing multiple sensors simultaneously and receiving overlapping answers, each sensor comes with an ID that is hard-coded and is unique to each sensor. This ID can contain hexadecimal digits and it is 10 digits long. When the user first uses the sensor, or when there multiple around and he/she wants to receive measurements from one of tehm can insert the unique sensor ID and then only that sensor will receive the instruction to perform the measurement. Figure 7.13 shows the user interface that the user inserts the ID. It must be noted that this value is saved in the application data and so the iuser only needs to insert the ID once.

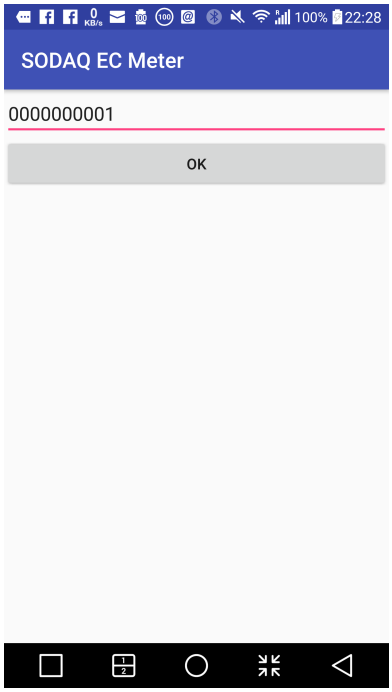

Figure 7.13: Android app: Register the ID of the sensor

7.2.3. Calibration of the sensor

The sensor comes out of the box without the need of calibration. Despite that, it can happen that the sensor gets physically damaged or corroded. In such cases, or at any given moment that the user wishes, the sensor can be calibrated.

The procedure of the calibration is very simple for the user. The only thing that he/she needs to do is to submerge the probe in a calibration fluid, that is provided with the sensor, of 1413μS/cm conductivity and press the calibration button, shown in Figure 7.14:

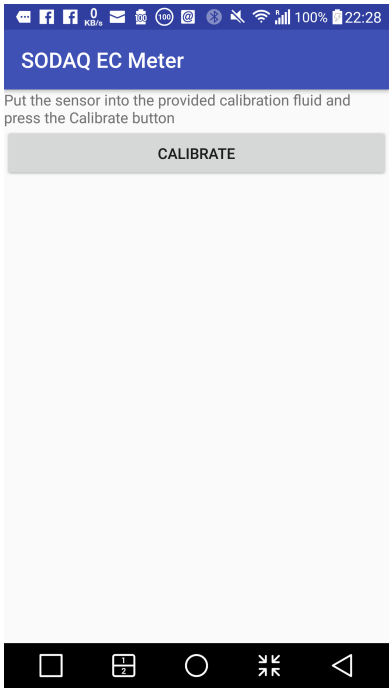

Figure 7.14: Android app: Calibration

7.2.4. More Data

This interface allows the user to acquire more data, in case they are useful in any way. From this interface the user can read the voltage of the probe, the resistance of the sample and the conductance of the sample. The button in this interface does exactly the same thing as the one on the main user interface. An image of this interface is shown in Figure 7.15:

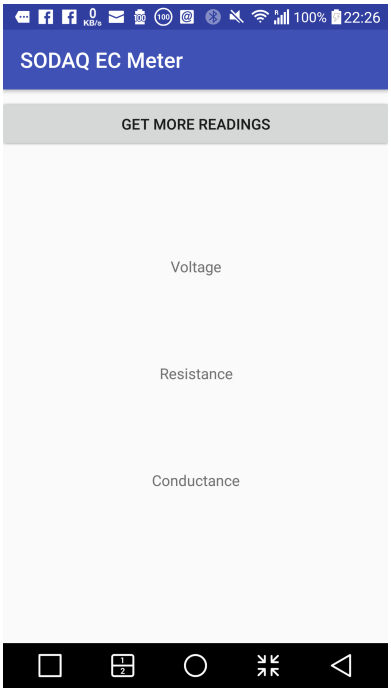

Figure 7.15: Android app: More data

7.3. System functionality

In order to to achieve as high accuracy as possible each conductivity measurement is the outcome of 100 individual conductance measurements. Those values are averaged and from that value, the cell constant is calculated and finally the conductance is calculated. During the experimentation phase it was determined that this number of samples is sufficient to minimize the fluctuation of the measurements. A measurement takes approximately 17 seconds. This time can be reduced, by reducing the samples, but it will have an impact on the stability of the measurement. This measurement scheme also has an impact on the battery consumption, but since the device can be recharged it does not pose as a problem. On stand-by the sensor works for approximately 6 days.

The calibration procedure is simple for the user, it basically consists of 100 conductance measurements again that are averaged out. Then using the revere calculation that is used to calculate the cell constant and with the conductance given (1413μS/cm) the "cell constant" is calculated.

The mathematical formula for that calculation is the following:

$$\left[\frac{1413}{conductance}\left(1+\frac{q_1}{conductance}\right)\right]-\frac{p_2}{conductance}$$

Where q_1 and pq_2 are calculated from the simulation results.

8

Testing and Proof of the functionality of the System

This chapter describes the testing performed on the probes and the results obtained.

At the moment of writing of the present report there have been two models of the sensor. The one shown in Figure 7.11 and the one shown in the figure below:

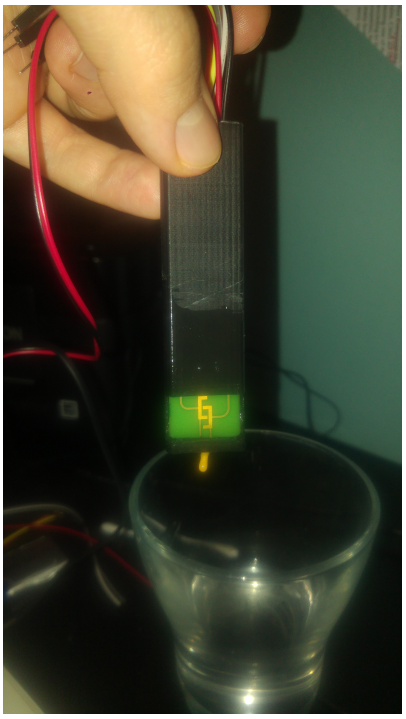

Figure 8.1: Second Prototype

Tests performed using the first prototype indicated improvements that were then applied on the second prototype.

8.1. First round of testing

There were two different measurement series. For each set of measurements, the probe was calibrated, using a calibration fluid of known conductivity 1413μS/cm.

The results of the first round of measurements are given in the following table:

Conductivity (μS/cm) (%)	Measured Conductivity (μS/cm)	Error(%)
151	160	6.6
242	231	4.4
480	491	2.3
1446	1447	0.1
3010	3062	1.7
8150	8399	3.1
13100	13539	3.4
21300	20824	2.2

Table 8.1: Resistance of various NaCl concentration solutions

One measurement is timed to last 4 seconds. In order to simulate the ageing of the probe, it was put into a sample of water that had extremely high conductivity (over 30.000μS/cm) for over a week, at which the signal was constantly applied on the probe. This corresponds to years of usage, assuming that the user will make 2-4 measurements per day.

After the probe was removed from the water sample, the probe was heavily corroded on the probe element that the signal is applied (Figure 8.2)

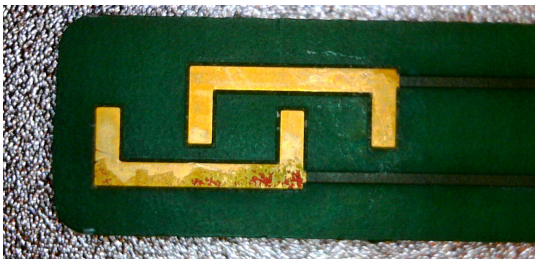

Figure 8.2: Corroded probe, after ageing simulation

Despite this damage, the probe was recalibrated, with the method described above and the results from the new set of measurement are shown in Table 8.2.

Conductivity (μS/cm) (%)	Measured Conductivity (μS/cm)	Error(%)
164	166	1.2
251	254	1.2
503	543	8
1472	1523	3.5
3130	3183	1.7
8290	8341	0.6
13230	13480	1.9
21500	21320	0.8

Table 8.2: Resistance of various NaCl concentration solutions

The findings of the second row of measurements shows that the (re-) calibration scheme, that was described previously can work. Also the fact that the probe can achieve such accuracy even after being subjected to such a tough testing process, concludes the discussion of the functionality of the design.

8.2. Second round of testing

The first round revealed that the probe actually corrodes when exposed for a long time to a highly conductive sample. For that reason the second prototype was ordered to be hard-gold plated. In order to check the scalability of the sensor two devices were assembled and tested.

In the first series of measurements the default calibration was used. The samples were also measured using the **Greisinger GMH 3431** and the comparison is made against those measurements. Tables 8.3 and 8.4 show the results obtained.

Greisinger (μS/cm)	Greisinger Temperature (μS/cm)	Sensor1 Conductivity	Sensor 1 Temperature	Error(%)
167.8	21.5	163	22.0	2.9
251	21.5	252	22.0	0.4
501	21.5	477	22.0	4.8
1462	22.1	1455	22.5	0.5
3090	21.7	3105	22.1	0.5
8250	21.8	8466	22.2	2.6
13170	22.1	13626	22.5	3.5
15360	21.9	15992	22.2	4.1
21700	21.8	21516	22.2	0.8

Table 8.3: Measurement set using the out-of-the-box calibration for device 1

Greisinger (μS/cm)	Greisinger Temperature (μS/cm)	Sensor 2 Conductivity	Sensor 2 Temperature	Error(%)
167.8	21.5	167	22.5	0.5
251	21.5	258	22.5	2.8
501	21.5	505	22.3	0.8
1462	22.1	1510	22.6	3.3
3090	21.7	3218	22.3	4.1
8250	21.8	8736	22.4	5.9
13170	22.1	14060	22.6	6.8
15360	21.9	16627	22.4	8.2
21700	21.8	22307	22.4	2.8

Table 8.4: Measurement set using the out-of-the-box calibration for device 2

The second round of measurements took place after the sensors were calibrated. The results can be seen on the Tables 8.5 and 8.6.

Greisinger (μS/cm)	Greisinger Temperature (μS/cm)	Sensor1 Conductivity	Sensor 1 Temperature	Error(%)
167.8	21.5	166	21.7	1.1
251	21.5	249	21.7	0.8
501	21.5	513	21.7	2.4
1462	22.1	1533	22.3	4.9
3090	21.7	3248	21.8	5.1
8250	21.8	8810	22.0	6.8
13170	22.1	114249	22.3	8.2
15360	21.9	16605	22.0	8.1
21700	21.8	22513	22.0	3.7

Table 8.5: Measurement set after calibration for device 1

Greisinger (μS/cm)	Greisinger Temperature (μS/cm)	Sensor 2 Conductivity	Sensor 2 Temperature	Error(%)
167.8	21.5	162	22.5	3.5
251	21.5	250	22.5	0.4
501	21.5	498	22.5	0.6
1462	22.1	1499	22.8	2.5
3090	21.7	3206	22.5	3.8
8250	21.8	8692	22.5	5.4
13170	22.1	13912	22.7	5.6
15360	21.9	16344	22.5	6.4
21700	21.8	21669	22.5	0.1

Table 8.6: Measurement set after calibration for device 2

In order to verify that the sensor can now resist corrosion, one of the sensors was submerged in a highly conductive water sample for more than a week. After this period of time there was no sign of corrosion on the sensor.

8.3. Conclusions

Looking at the results obtained using the two different prototypes, it is obvious that the accuracy goal of accuracy of 10% over the whole spectrum between 0 and 20.000μS/cm is achieved. For the most measurements accuracy was way higher than the set goal.

It can be also seen that the calibration out-of-the-box provides excellent results and those are achieved simply by using the results of the simulations.

Another important outcome of the tests is that the design can work for multiple sensors and that the accuracy goal can be achieved for all of them.

9

Conclusions and future work

Looking at the results obtained and reflecting on the goals that were set in the beginning of the project, it can be said that all of them were met to a satisfying degree.

The system is portable, highly accurate, simple to use, and the cost of 1 board, out of a batch of 100 is approximately 30€. The current system works very well when it comes out of the box, while it can be recalibrated when the user finds it fit in a very simple and straightforward way. For the manufacturer the assembly and programming work is minimized, reducing the cost in hardware, as well as in labour.

The results presented on the previous chapter showed high precision when the measurements were compared to an expensive conductivity sensor, that is available in the market costing 250€.

While the project was in development phase there were various issues that came up and dealt with:

What is the most suitable method to be used for measuring conductivity in accordance to the requirements of the project?

What are the important features that characterise the sensor?

How does the interdigitated probe behaves?

What is the best way to measure the voltage difference between the terminals of the probe?

What is the impact of the temperature and how can it be utilized to measure conductivity accurately?

What kind of temperature sensor would be the most appropriate for the project?

How well does the system comply with the requirements?

All those questions were answered in the previous chapters. The results obtained were not always easily explicable. Some findings could be further investigated in future works. The greatest, possibly question that needs further investigation, but is outside of the scope of the present work is the behaviour of the planar interdigitated electrodes and the curve of the cell constant when plotted against conductivity. An explanation of this image was attempted, but in an intuitive level.

More work can be done using the present sensor. For example, by upgrading the application, the user can upload the conductivity values to a server or a cloud, along with a GPS signature and a time-stamp. With those data, a map of the values of conductivities can be created easily and there can be an analysis for patterns. This can help identify either pollution and other phenomena taking place in a the habitat.

It is also important to point out that there are other promising techniques to be investigated in the future, such as the microwave spectroscopy. With microwave spectroscopy it is possible to identify molecules and have an even more clear image on the composition of samples under investigation.

Finally the outcome of the present thesis, with some modifications and further testing can go to the stage of production of a robust sensor that can help society to monitor the environment in a reliable and accurate way and improve the income and production of individuals around the globe.

A

Appendix: MATLAB scripts

A.1. Impedance analyser script

```
% Script to sweep and read out data from Agilent 4294A Impedance Analyzer
% Anastasopoulos Ioannis, 2016
% based upon the generic Visa code http://www.mathworks.com/matlabcentral/
    fileexchange/28887-capturing-a-waveform-from-an-agilent-oscilloscope-over-a-
    standard-visa-interface
% for more machine commands, have a look in the 4294A Programming Manual

% Make sure to have installed and configured Keysight Connection Expert
% before running this code.

%% Interface configuration and instrument connection

visaObj = visa('agilent','TCPIP0::192.168.2.10::5025::SOCKET');% Insert the right IP
    adress of the machine
visaObj.InputBufferSize = 10000000;
visaObj.Timeout = 5;% This should be long enough to transfer all measurement data. 5
    seconds was enough for 201 sweep samples
visaObj.ByteOrder = 'littleEndian';
fopen(visaObj);

fprintf(visaObj,'TRGS BUS');%Trigger via LAN

%%

% Trigger
fprintf(visaObj,'*TRG');
pause(10) % Pause during sweep time

% Get frequency vector freqs
outp=query(visaObj,'OUTPSWPRM?');
freqs=str2num(outp);

outp=query(visaObj,'OUTPDTRC?');
temp=str2num(outp);
Imp=temp(1:2:end);

R=real(Imp)

```

```
mkdir measurements-probe1_backplane/capacitance;
mkdir measurements-probe1_backplane/conductance;

figure(1)
scatter(freqs,R)
D = [freqs; R];
fileID = fopen('measurements-probe1_backplane/conductance/0.txt','w');
fprintf(fileID,'%f %1.20f\n',D);
fclose(fileID);
fclose(visaObj);
delete(visaObj);
clear visaObj;
```

A.2. Cell Constant calculator script

```
clc;
s = 1800;
w = 650;
L = 950;
N = 4;
n = w/(w+s);
if N == 2
    k = s/(s+w);
else
    k = cos(pi*n/2)
end
fun = @(x,c) 1./sqrt((1-x.^2).*(1-(c*x).^2));
K1 = integral(@(x)fun(x,k),0,1)
fun1 = @(x,c) 1./sqrt((1-x.^2).*(1-(x.^2)+(c*x).^2));
K2 = integral(@(x)fun1(x,k),0,1)
cc = 2*K1/K2/L/(N-1)*10
```

A.3. Curve fitting script

```
clc;
formatSpec = '%f %f';
name = strcat('\cc-conductance-0to3000uS.txt');
fileID = fopen(name, 'r');
sizeA = [2 Inf];
A = fscanf(fileID, formatSpec,sizeA);
fclose(fileID);
B = transpose(A);
f = fit(B(:, 1),B(:, 2), 'rat11')
plot(f,B(:, 1),B(:, 2));
xlabel('Conductance(uS)');
ylabel('Cell Constant');
k = B(1,1)/10
```

A.4. Design iteration script

```
clc;
mphopen('D:\ganastasopoulo\Desktop\Probe_simulation2.mph');
pathname = 'D:\ganastasopoulo\Desktop\Simulation_results\';
sim_num = 0;

for i = 1:5
    w = 200+i*150;
```

```
8       wvalue = strcat(num2str(w),'[um]');
9       model.param.set('w',wvalue);
10      for j = 0:5
11          S2 = 200+j*150;
12          S2value=strcat(num2str(S2),'[um]');
13          model.param.set('S2',S2value);
14          for k = 0:10
15              S1 = 1000+k*200;
16              S1value = strcat(num2str(S1),'[um]');
17              model.param.set('S1',S1value);
18              for m = 0:10
19                  l = 500+m*150;
20                  lvalue = strcat(num2str(l),'[um]');
21                  model.param.set('l',lvalue);
22                  model.sol('sol1').run();
23                  name = strcat('w=',num2str(w),' S2=',num2str(S2),' S1=',num2str(S1),
                        ' l=', num2str(l));
24                  filename = strcat(pathname,name,'.txt');
25                  model.result.export('plot1').set('filename',filename);
26                  model.result.export('plot1').run();
27                  sim_num = sim_num+1;
28                  Message = strcat('Number of completed simulations: ', num2str(
                        sim_num))
29              end
30          end
31      end
32  end
```

B

Appendix: Tables

B.1. Brix Conversion table

Salt g/kg	Refraction index	Brix (%)
0	13.330	0
10	13.348	1.3
20	13.366	2.5
30	13.383	3.7
40	13.400	4.8
50	13.418	6.0
60	13.435	7.2
70	13.453	8.4
80	13.470	9.5
90	13.488	10.6
100	13.505	11.7
110	13.523	12.8
120	13.541	14.9
130	13.558	15.1
140	13.576	16.1
150	13.594	17.2
160	13.612	18.4
170	13.630	19.5
180	13.648	20.6
190	13.666	21.7
200	13.684	22.7
210	13.703	23.8
220	13.721	24.9
230	13.740	26.0
240	13.759	27.1
250	13.778	28.1
260	13.797	29.2

Table B.1: Brix converted to Refraction index and salt concentration

Bibliography

[1] URL https://www.vernier.com/products/sensors/ion-selective-electrodes/cl-bta/. Chloride Ion-Selective Electrode.

[2] Commercial ec meter. URL https://www.bol.com/nl/p/digitale-ec-tds-en-temperatuur-meter/9200000058717958/?Referrer=ADVNLGOO002027-G-36371376386-S-69259941884-9200000058717958&gclid=CjOKCQjwnubLBRC_ARIsAASsNNnQjgylzazRNR1hpFww96nXWjks4VWJhEicD2xSn9HwcmgXMJAvDWcaAptiEALw_wcB.

[3] Mass transport. URL http://www.ceb.cam.ac.uk/research/groups/rg-eme/teaching-notes/mass-transport.

[4] Determination of chloride ion concentration by titration (mohr's method). URL http://www.outreach.canterbury.ac.nz/chemistry/documents/chloride_mohr.pdf.

[5] URL http://www.kno3.org/en/product-features-a-benefits/potassium-nitrate-and-saline-conditions/effect-of-salinity-on-crop-yield-potential-.

[6] Ametherm. URL https://www.ametherm.com/blog/thermistors/temperature-sensors-thermistors-vs-thermocouples.

[7] Autolab. Equivalent circuit models. 2011. URL http://www.ecochemie.nl/download/Applicationnotes/Autolab_Application_Note_COR04.pdf.

[8] John J. Barron and Colin Ashton. The effect of temperature on conductivity measurement. *A Practical Guide to Accurate Conductivity Measurement*.

[9] M. Baumgartner and R. J. Bakker. Raman spectroscopy of pure h2o and nacl-h2o containing synthetic fluid inclusions in quartz—a study of polarization effects. *Mineralogy and Petrology*, 95(1):1–15, Jan 2009. ISSN 1438-1168. doi: 10.1007/s00710-008-0028-z. URL https://doi.org/10.1007/s00710-008-0028-z.

[10] Dr. Axel W. Bier and Hach-Lange. Introduction to ion-selective measurement. 2009. URL https://us.vwr.com/assetsvc/asset/en_US/id/7979405/contents.

[11] Sir Edward Bullard. URL http://www.kayelaby.npl.co.uk/general_physics/2_7/2_7_9.html.

[12] Cole-Palmer. Conductivity theory and technical tips. 03 2017. URL https://www.coleparmer.com/tech-article/conductivity.

[13] Electronics-tutorials. URL http://www.electronics-tutorials.ws/io/io_3.html.

[14] Emerson. Theory and applications of conductivity. 01 2010. URL http://www.emerson.com/documents/automation/68442.pdf.

[15] Christopher Fry, Stephen Langley E. N., and Stephen Langley. Ion-selective electrodes for biological systems. 2004.

[16] Klaus Grasshoff and Klaus Kremling andManfred Ehrhardt. Methods of seawater analysis. 2009.

[17] Masaki Hayashi. Temperature-electrical conductivity relation of water for environmental monitoring and geophysical data inversion. *Environmental Monitoring and Assessment*, 96(1):119–128, Aug 2004. ISSN 1573-2959. doi: 10.1023/B:EMAS.0000031719.83065.68. URL https://doi.org/10.1023/B:EMAS.0000031719.83065.68.

[18] Jaromír Hubálek. Iterative precise conductivity measurement with ides. *Sensors*, 2015.

[19] Thermocouple info. URL http://www.thermocoupleinfo.com/.

[20] Gamry Instruments. Introduction to electrochemical impedance spectroscopy. URL https://www.gamry.com/assets/Uploads/Basics-of-Electrochemical-Impedance-Spectroscopy.pdf.

[21] Sanjay Kumar Jain and Vandana Soni. Bentley's textbook of pharmaceutics. 2012.

[22] I. Kan and M.Rapaport-Rom. Regional blending of fresh and saline irrigation water: Is it efficient? *Water Resources Research*, 2012.

[23] B. Kapilevich and B. Litvak. Microwave sensor for accurate measurements of water solution concentrations. pages 1–4, Dec 2007. ISSN 2165-4727. doi: 10.1109/APMC.2007.4554682.

[24] O. Korostynska, A.Mason, and A.I. Al-Shamma'a. Monitoring pollutants in wastewater: Traditional lab based versus modern real-time approaches. *Smart Sensors for Real-Time Water Quality Monitoring*.

[25] O.I. Mamayev. Temperature-salinity analysis of world ocean. 1975.

[26] Stanley E. Manahan. Fundamentals of environmental chemistry, third edition. 2008.

[27] Jérôme Mathieu and Patrick Schweitzer. Measurement of liquid density by ultrasound backscattering analysis. *Measurement Science and Technology*, 15(5):869, 2004. URL http://stacks.iop.org/0957-0233/15/i=5/a=012.

[28] W. Olthius, W.Streekstra, and P. Begveld. Theoretical and experimental determination of cell constants of planar-interdigitated electrolyte conductivity sensors. *Sensors and Actuators*, 1995.

[29] Omega. URL http://www.omega.com/prodinfo/thermistor.html.

[30] M. Ortoneda-Pedrola, O. Korostynska, A. Mason, and A. I. Al-Shamma'a. Real-time sensing of nacl solution concentration at microwave frequencies using novel ag patterns printed on flexible substrates. *Journal of Physics: Conference Series*, 2013.

[31] F. Pino, H. Barros, and L. Sajo-Bohus. Determination of multiple compton scattering fractions in gamma densitometry by monte carlo simulation. *IEEE Transactions on Nuclear Science*, 61(2):870–876, April 2014. ISSN 0018-9499. doi: 10.1109/TNS.2014.2300504.

[32] R. Prien. Technologies for new in situ chemical sensors. pages 1–6, June 2007. doi: 10.1109/OCEANSE.2007.4302222.

[33] B. K. Roy, K. V. Santhosh, R. K. Bharti, and R. Kanthmani. Labview implementation of liquid density measurement using ultrasonic transducers. pages 1–4, Feb 2014. doi: 10.1109/ICICES.2014.7034194.

[34] R. Eberhardt S. Seitz, P. Spitzer. New primary setup for conductivity sensor calibration in pure water between 5.5 us m-1 and 15 ms m-1. 2013.

[35] H. P. Schwan. Electrode polarization impedance and measurements in biological materials*. *Annals of the New York Academy of Sciences*, 148(1):191–209, 1968. ISSN 1749-6632. doi: 10.1111/j.1749-6632.1968.tb20349.x. URL http://dx.doi.org/10.1111/j.1749-6632.1968.tb20349.x.

[36] J. Soto, I. Campos, and R. Martínez-Máñez. Monitoring wastewater treatment using voltammetric electronic tongues. *Smart Sensors for Real-Time Water Quality Monitoring*.

[37] Robert P. Sutton, Stuart A. Cox, James F. Lea, and O. Lynn Rowlan. Guidelines for the proper application of critical velocity calculations. *SPE Production & Operation*, 25(2), 05 2010. doi: 10.2118/120625-ms.

[38] Linear Technologies. URL http://cds.linear.com/docs/en/datasheet/1968f.pdf.

[39] Innovative Sensor Technology. . URL https://www.azom.com/article.aspx?ArticleID=5573.

[40] Linear Technology. . URL http://www.linear.com/solutions/7161.

[41] Topac. URL http://www.topac.com/salinity_brix.html.

[42] David G. Watson. Pharmaceutical analysis e-book: A textbook for pharmacy students and pharmaceutical chemists. 2015.

[43] Frank Thompson Werner. Electromagnetic characterization of a pcb salinity sensor. Master's thesis, Auburn University, 2016. URL https://etd.auburn.edu/bitstream/handle/10415/5260/Frank_Werner_Thesis.pdf?sequence=2.

[44] Xiangen Wu, Wanjun Lu, Wenjia Ou, Marie-Camille Caumon, and Jean Dubessy. Temperature and salinity effects on the raman scattering cross section of the water oh-stretching vibration band in nacl aqueous solutions from 0 to 300c. *Journal of Raman Spectroscopy*, 48(2):314–322, 2017. ISSN 1097-4555. doi: 10.1002/jrs.5039. URL http://dx.doi.org/10.1002/jrs.5039.

[45] Yong Zhao, Xinyuan Zhang, Tingting Zhao, Bo Yuan, and Shuo Zhang. Optical salinity sensor system based on fiber-optic array. *IEEE SENSORS JOURNAL*, 9(9), 09 2009.

[46] Øyvind Aasen Tengesdal. Measurement of seawater refractive index and salinity by means of optical refraction. 2012.